DEVELOPMENT OF NEURAL NETWORK BASED ALGORITHM OF ACTIVE ANKLE PROSTHESIS USING GAIT ANALYSIS DATA

by

Ahmet Doğukan Keleş

B.Sc., Mechatronics Engineering, Yıldız Technical University, 2013

Submitted to the Institute of Biomedical Engineering
in partial fulfillment of the requirements
for the degree of
Master of Science
in
Biomedical Engineering

Boğaziçi University
2017

ACKNOWLEDGMENTS

First and foremost, I would like to thank my supervisor, Prof. Dr. Can A. Yücesoy, for guiding and supporting me over the years. His insightful comments and directions have guided me to be successful both in my research and in my personal life.

I would like to thank my family and friends who have supported me throughout the entire process by giving me the courage and the help to reach my goals.

Finally, I would like to express my gratitude to my dearest, Cemre Su, to whom I dedicate this dissertation, for her love, encouragement, patience, and support that made everything possible.

ACADEMIC ETHICS AND INTEGRITY STATEMENT

I, Ahmet Doğukan Keleş, hereby certify that I am aware of the Academic Ethics and Integrity Policy issued by the Council of Higher Education (YÖK) and I fully acknowledge all the consequences due to its violation by plagiarism or any other way.

Name : Signature:

_____ _____

Date:

_____

ABSTRACT

DEVELOPMENT OF NEURAL NETWORK BASED ALGORITHM OF ACTIVE ANKLE PROSTHESIS USING GAIT ANALYSIS DATA

Amputation is the removal of a part or all of a limb due to disease, accident or trauma and it has a large incidence rate. For example, in the United States, an average of 500 people loses at least one limb every day, approximately 65% of which is comprised of lower limb amputations. Since energetically active prostheses are costly, amputees usually continue with their daily lives using a wheelchair or a passive prosthesis. The aim of this study is to determine the optimum sensor needs for an active ankle prosthesis and to develop an algorithm suitable for this sensor infrastructure. In the long run, design of a device that is both easy to use and financially feasible is aimed at and the present work is central to that aim. In this context, three neural networks structures with different inputs were developed to facilitate ankle movement and their performances were evaluated. The results show that if a device in which only EMG signals are to be used as network inputs, a total of 5 signals should be collected from different muscles that are responsible for hip, knee and ankle movements. The results also show that, if the use of a smaller number of EMG sensors is preferred, it is necessary to incorporate also a force or torque feedback into the system. In such application, three EMG signals collected from tibialis anterior, soleus and gastrocnemius medialis muscles were shown to suffice. These findings shed an important light to our understanding of the number and kind of sensor inputs necessary for an active ankle prosthesis requirements of which can be variable depending on the amputation level of the patient and the mechanical design flexibility.

Keywords: Electromyography, EMG, Neural Network, Active Ankle Prosthesis.

ÖZET

YÜRÜME ANALİZİ VERİLERİ KULLANILARAK AKTİF AYAK BİLEĞİ PROTEZİNİN SİNİR AĞI TABANLI ALGORİTMASININ GELİŞTİRİLMESİ

Hastalık, kaza veya travma nedeniyle, bir uzvun tamamının ya da bir kısmının kesilmesi işlemine ampütasyon denir ve oldukça sık uygulanmaktadır. Örneğin, Amerika Birleşik Devletleri'nde her gün ortalama 500 insan en az bir uzvunu kaybederken, bunların yaklaşık olarak %65'i alt ekstremite ampütasyonlarından oluşur. Enerji tüketimi açısından aktif protezlerin maliyetleri yüksek olduğu için, ampüte insanlar tekerlekli sandalye veya pasif bir protezi kullanarak günlük yaşamlarına devam etmektedir. Bu çalışmanın amacı, aktif bir ayak bileği protezi için optimum sensör gereksinimlerini belirlemek ve bu sensör altyapısına uygun bir algoritma geliştirmektir. Uzun vadede, hem kullanımı kolay hem de mali açıdan uygulanabilir olan bir cihazın tasarlanması amaçlanmaktadır ve mevcut çalışma bu amaca yöneliktir. Bu kapsamda, ayak bileği hareketlerinin tahmin edilebilmesi için farklı girişlere sahip üç sinir ağı yapısı geliştirilmiş ve performansları değerlendirilmiştir. Sonuçlar, sadece elektromiyografi (EMG) sinyallerinin ağ girişi olarak kullanılması durumunda, kalça, diz ve bilek hareketlerinden sorumlu farklı kaslardan toplam 5 adet sinyalin toplanması gerektiği göstermiştir. Sonuçlar ayrıca, eğer daha az sayıda EMG sensörünün kullanılması tercih edilirse, sisteme bir kuvvet veya tork geribildirimi eklemek gerektiğini göstermiştir. Böyle bir uygulamada, tibialis anterior, soleus and gastrocnemius medialis kaslarından toplanan üç EMG sinyalinin yeterli olduğu gösterilmiştir. Bu bulgular, hastanın ampütasyon seviyesine ve mekanik tasarım esnekliğine göre, aktif bilek protezinin ihtiyaç duyduğu sensör miktarının ve sensör tiplerinin belirlenmesinde yol gösterici olmuştur.

Anahtar Sözcükler: Elektromiyografi, EMG, Sinir Ağları, Aktif Ayak Bileği Protezi.

TABLE OF CONTENTS

LIST OF FIGURES

LIST OF TABLES

LIST OF SYMBOLS

x	Neural network input
y	Neural network output
w	Weight of a neuron in a neural network
b	Bias of a neuron in a neural network
θ	Transfer function of a neuron in a neural network

LIST OF ABBREVIATIONS

EMG	Electromyography
CNS	Central Nervous System
MU	Motor Unit
AP	Action Potential
MUAP	Motor Unit Action Potential
sEMG	Surface Electromyography
TA	Tibialis Anterior
SOL	Soleus
GAM	Gastrocnemius Medialis
PL	Peroneus Longus
RF	Rectus Femoris
VM	Vastus Vedialis
BF	Biceps Femoris
GM	Gluteus Maximus
GRFs	Ground Reaction Forces
TDNN	Time Delay Neural Networks
TYPE I_{TP-}	TYPE $I_{\text{Trained Without the Protocol}}$
TYPE I_{TP+}	TYPE $I_{\text{Trained With the Protocol}}$
TYPE II_{GRF-}	TYPE $II_{\text{Without Ground Reaction Forces Inputs}}$
TYPE III_{GRF-}	TYPE $III_{\text{Without Ground Reaction Forces Inputs}}$
TYPE III_{GRF+}	TYPE $III_{\text{With Ground Reaction Forces Inputs}}$

1. INTRODUCTION

Along with the exciting and revolutionary technological developments in recent years, many innovative systems in the field of assistive robotics are advanced to restore legged locomotion for individuals suffering from lower limb amputations. As first examples of assistive systems, energetically passive prosthetic devices have been in use for many years. These systems, which are still being used successfully, are practical tools to enable functional recovery of gait pathologies stemming from many conditions owing to their relative simplicity, low cost, and robust design. Therefore, while many developments have been made in lower limb prostheses, the majority of commercial lower limb prostheses are passive types. The advanced composites used in these lightweight devices store energy during controlled dorsiflexion and plantar flexion, and release the stored energy during powered plantar flexion like the Achilles tendon [1–3]. Although such passive-elastic behavior provides a good approximation to the ankle's function during slow walking, normal and fast walking require external energy, which cannot be fulfilled by passive devices. The inherent shortcomings of these devices are their inability to generate mechanical power, their failure to autonomously adapt to the user's changing needs, and the lack of sensory feedback that they provide to the user regarding the status of the limb and of the device. Each of these shortcomings is required to be resolved for a seamless cognitive and physical interaction between the device and the user [4–6].

Advancements in actuation, energy storage, miniaturized sensing, automated pattern recognition and embedded computational technology have led to the development of a number of robotic devices for the assistance and restoration of human locomotion [6]. In the last few decades, researchers have been developing powered lower limb prostheses to assists normal gait beyond slow walking speeds. Some of these are size and weight vise comparable to actual human ankle-foot and have the elastic energy storage, motor power, and battery energy to provide for a day's typical walking activity [7, 8]. On top of many engineering challenges existing regarding

the mechanical design of such devices, additional difficulties to be overcome include control algorithms of these devices to function in concert with the user's remaining sensory-motor control system.

Skin surface electromyogram (EMG), generated by muscle cells during muscle contractions, is often used in order to control the assistive robotic systems according to the user's intention since this directly reflects the user's muscle activity level in real time [9, 10]. Owing to the developments in sensory systems, EMG signals can be easily recorded and classified by embedded systems to make a precise prediction of the intended motion of a joint in terms of position and moment change [11].

While various modeling methods are being used for EMG classification, the Hill's muscle model [12], biomimetic models, neural networks, fuzzy logic and genetic algorithms are the most common ones utilized [13]. Sepulveda et al [14] developed a neural network with the back propagation algorithm to model the relationship between muscle activity and joint motion. To predict the position and moment change in the hip, knee, and ankle, EMG signals from 16 muscles were used as network inputs. In the later years, Savelberg et al [15, 16] also used an artificial neural network approach based on a back-propagation algorithm to predict cat soleus muscle force by using only EMG signals. Similarly, Huang et al [17] identified locomotion modes using a pattern recognition algorithm based on EMG signals, and Zhang et al [18] designed a feed-forward neural network model to control the ankle exoskeleton using EMG signals from five below-knee muscles.

In other studies carried out in parallel, different algorithmic structures were developed to predict joint movements. In these studies, additional estimation-making parameters were added along with EMG signals and used for mechanical control purposes. Kiguchi et al [19] proposed an EMG based impedance control method for an upper limb power-assist exoskeleton robot. Real-time force and torque feedback signals collected from sensors were used in addition to EMG signals from 16 muscles to control the robot in accordance with the user's motion intention. Sup et al [20] designed a control structure for an electrically powered knee and ankle prosthesis using a load cell

to measure the sagittal socket interface moment above the knee joint, a custom sensorized foot to measure the ground reaction force at the heel and ball of the foot, and commercial potentiometers and load cells to measure joint positions and torques. Herr et al [8] developed a myoelectric-driven, finite state controller for a powered ankle-foot prosthesis that modulates both impedance and power output during stance. The developed system employed both position and force inputs measured local to the external prosthesis, and myoelectric inputs measured from residual limb muscles. Local prosthetic sensing was used to develop two finite state controllers to produce biomimetic movement patterns for level-ground and stair descent gaits, while myoelectric signals were used as control commands to manage the transition between these finite state controllers. Fleischer et al [9] proposed a real-time controller for a powered leg orthosis using a knee angle sensor, six EMG sensors and a force sensor in series with the linear actuator.

The most crucial part of the assistive robotic systems such as active ankle prosthesis is the main algorithm that operates these devices. Although recent studies have made important contributions to the improvement of these prostheses, there are points that need to be reconsidered for the development of a low-cost device. Especially, there are inconsistencies regarding the number of EMG signals used as inputs to running algorithms and from which muscles they are collected.

In this context, the uncertainties about EMG requirement and usage are needed to be eliminated for the development of a system in which unnecessary sensor usage would be avoided. Because, EMG sensors are easily affected by external and environmental effects [21], therefore, redundant amount use of these sensors may cause misleading results in outputs of the algorithm. Furthermore, unneeded use of these sensors which are being used by being stuck to the body may increase the user discomfort in the long-term usage.

Studies and commercial products also show that using force and/or torque feedback in addition to EMG signals as system inputs enables stability in the system output [8,9,19,20]. However, since these sensors are expensive items that cause an increase

in the prosthesis' price, it is needed to find the most effective neural network structure that using nothing but EMG signals as input. Therefore, by making a comparison between two different algorithms in terms of the force and torque feedback integration, not only comfortable but also low-cost device's algorithm can be constructed.

Transtibial amputations differ by the area where the limb has been cut off. In some patients, amputation is performed near the knee, while in others it is applied to a region close to the ankle. For this reason, the muscles left in the residual limbs and the EMG signals' quality varies from patient to patient. The differences in amputation levels can be easily observed from the soleus muscles' condition. If the transtibial amputation was applied to a place near to the knee, then recording an accurate EMG signal from the soleus muscle, which is widely used in such system's algorithms, may not be possible. In this context, algorithms which have same methods and structures but different from each other in terms of the use of soleus muscle's EMG signal can provide a flexibility for the development of active ankle prosthesis which can be used by amputees with different level amputations.

1.1 Human Ankle Biomechanics

Level-ground gait cycle begins with the heel strike and ends with the next heel strike of the same foot [22]. Mainly, it is divided into two phases: (1) *Stance phase* is the part which the foot remains in contact with the ground. It begins with the moment the heel touches the ground and ends when the same foot is lifted off the ground. The stance phase constitutes about 60 percent of the gait cycle. (2) *Swing phase* is the part, during which the foot is not in contact with the ground and swings in the air. The swing phase constitutes about 40 percent of the gait cycle [4, 5]. The phases of a gait cycle detailed above are shown in Figure 1.1.

According to Shultz et al [24], the stance phase can be divided into four sub-phases: (1) Heel strike, (2) loading response, (3) mid stance and (4) terminal stance. High tibialis anterior muscle activities are observed during the *heel strike* and *the*

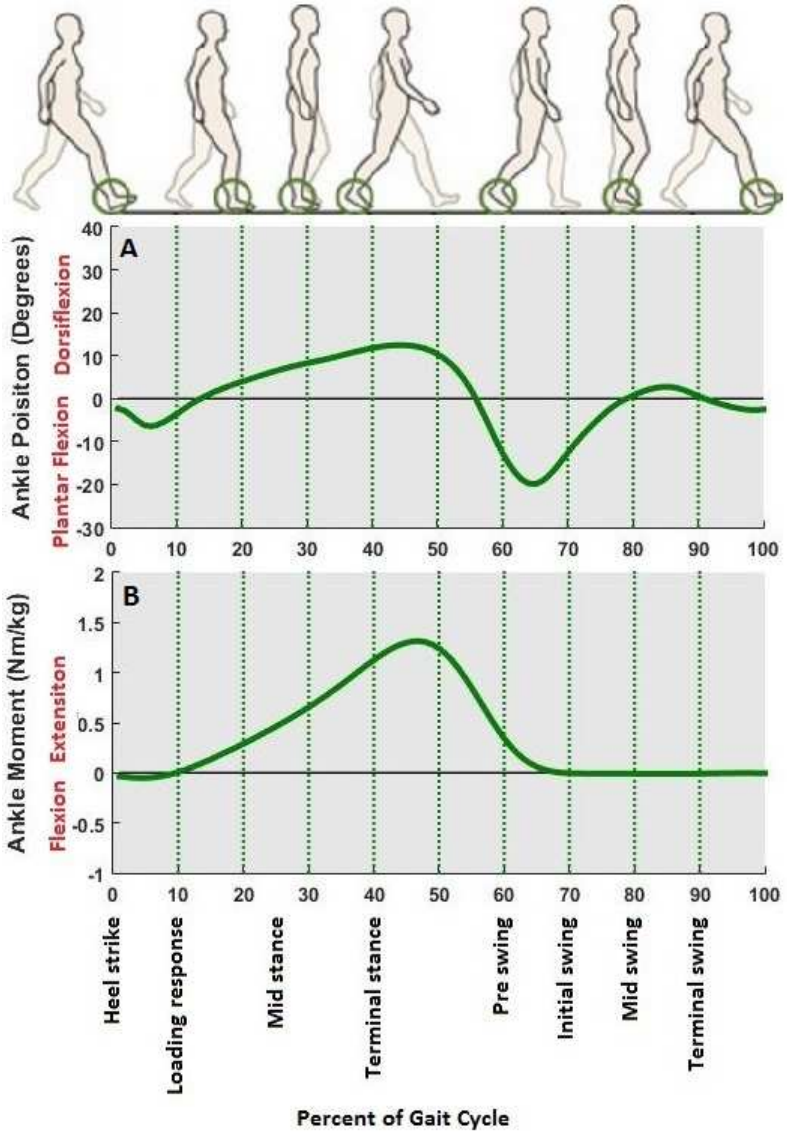

Figure 1.1 Ankle Position and Moment Change during Gait Cycle [23].

loading response while plantar flexor muscles, gastrocnemius and soleus, play crucial roles during *mid stance* and *terminal stance* sub-phases [25].

Heel strike (initial contact), is a short period of the gait, which begins at the moment the heel of the leading foot touches the ground. The hip and the knee are flexed at 20-30 degrees and 0-5 degrees, respectively. The ankle moves from a neutral position to plantar flexed position with the eccentric contraction of tibialis anterior [26, 27]. Although this is a momentary posture, it is significant because of its influence on subsequent knee action [28].

Loading response (foot flat), occupies about 12 percent of the gait cycle. It begins with initial floor contact and continues till the foot is lifted for the swing. The foot comes in full contact with the floor and body weight is fully transferred onto the stance limb [28]. The foot drops to 5-10 degrees plantar flexion and the knee are initiated to 15-20 degrees flexion. Little change in thigh position occurs during the loading response, the hip moves slowly into extension [26, 27].

Mid stance, represent the 12 to 31 percent of the gait cycle. It begins when the foot leaves the ground and continues as the body weight travels along the length of the foot until it is aligned over the forefoot. Advancement of the body and limb over a stationary foot is the functional objective of this gait phase [28]. In mid-stance, the hip moves from 10 degrees of flexion to extension which allows the trunk to remain erect while the limb becomes more vertical. The knee reaches maximal flexion and then begins to extend. The ankle becomes supinated and dorsiflexed to 5 degrees [26, 27].

Terminal stance (heel off) begins with heel rise and ends when the contralateral foot contacts the ground. Terminal stance occurs from the 31 to 50 percent periods of the gait. Forward fall by moving the body weight ahead of the forefoot to generate a propulsive force is the primary objective [28]. 10-20 degrees of hip hyperextension can be seen while the knee becomes passively flexed to 0-5 degrees because of forwarding alignment of the body. The ankle supinates and plantar flexes to 0-10 degrees [26, 27].

According to Shultz et al [24], the swing phase can be divided into four subphases: (1) Pre swing, (2) initial swing, (3) mid-swing and (4) terminal swing. During *initial swing*, *mid swing* and *terminal swing* phases, high muscle activities of tibialis anterior is observed, while gastrocnemius and soleus muscle play a critical role during *pre-swing* phase [25].

Pre swing (toe off), describes the instantaneous point in the gait when the leading foot leaves the ground. It occurs from the 50 to 62 percent of the gait cycle [28]. The hip loses extension and it is initiated to its natural position. The knee is passively flexed to 30-40 degrees. There is a rapid ankle plantar flexion to 15-20 degrees [26, 27].

Initial swing (early swing), is one-third of the swing period, from the 62 to 75 percent periods of the gait cycle. It begins the moment the foot leaves the ground and continues until maximum knee flexion occurs when the swinging extremity is direct to the body and directly opposite the stance limb. Clearance of the leading limb's foot off the ground is the primary objective of this phase [28]. The hip extends to 10-15 degrees rapidly from its neutral position. The knee flexes to 40-70 degrees for toe clearance of the floor and the ankle goes from plantar flexion to dorsiflexion, to end in a neutral position [26, 27].

Mid swing begins following maximum knee flexion and ends when the tibia is in a vertical position, which occurs from the 75 to 87 percent of the gait cycle [28]. The hip flexes to 25-30 degrees and the ankle becomes dorsiflexed. The knee flexes 60 degrees but then extends approximately 25-30 degrees [26, 27].

Terminal swing is the final phase of the gait cycle in which the tibia passes beyond perpendicular and the knee fully extends in preparation for the next heel strike [25]. The 30 degrees of hip flexion and dorsiflexed ankle attained in mid-swing is maintained. Extension of the knee to its natural neutral (0 or -5 degrees) continues under active control [26, 27].

Although the total range of the ankle joint motion approaches 90 degrees [29], the entire range of ankle motion used during walking is about 30 degrees. As shown in Figure 1.1, at heel-strike the ankle is slightly plantarflexed and as the body moves over the supporting foot, the ankle starts dorsiflexion. Just prior to pre-swing, the ankle once again becomes plantar flexed. During the swing phase, there is a second wave of dorsiflexion, which ensures clearance between the toes and ground. Towards the end of the swing phase, the ankle becomes plantar flexed prior to heel-strike [29–31].

The ankle moment variation during the gait is demonstrated in Figure 1.1. To provide a controlled foot rotation and avoiding foot to slip, dorsiflexion moment is generated in the heel strike phase. When the foot is flat, in the loading response phase, an extension moment is increased with the contractions of plantar flexor muscles;

consequently, the body starts to move forward. Extension moment increase in the ankle continues until the end of the terminal swing phase. Before the pre-swing phase, moment starts to decline and along the swing phase moment variation in the ankle does not occur [32–34].

1.2 Electromyography Signal

EMG is an electrodiagnostic procedure used for recording and evaluating the electrical activity of skeletal muscles [35] and EMG signal is an electrophysiological signal that represents the electrical activity generated when skeletal muscles contract and relax [36]. EMG signal has been extensively studied and applied in areas like sports training, gait and posture analysis [37], physical therapy [38], rehabilitation [39] and prosthesis [6, 40].

The central nervous system (CNS) controls muscle contractions and relaxations by carrying the electrical stimulations from the brain to target muscle [41]. A skeletal muscle consists of multiple bundles of cells called muscle fibers that are innervated by a single alpha spinal motor neuron, which is situated in the spinal cord. The motor neuron and all the muscle fibers compose the smallest functional unit, motor unit (MU), to describe the neural control of the muscular contraction process (Figure 1.2). When an MU is electrically activated, an electrical potential called action potential (AP) is generated and carried from the motor neuron to the target muscle [21, 42, 43]. Generated APs emerge at the neuromuscular junction in the middle of the muscle body and propagate along all muscle fibers. The repetitive firing of an MU creates a train of a pulse, which is called motor unit action potential (MUAP) [44]. The temporal summation of these electrical activities created by each MU is the EMG signal [45].

There are two types of EMG: (1) intramuscular EMG and (2) surface EMG (sEMG) [47]. Intramuscular EMGs are recorded by invasive electrodes like a monopolar or concentric needle electrodes, which are inserted through the skin into the target muscle tissue. Although it is the most accurate way to record the muscle activity, a

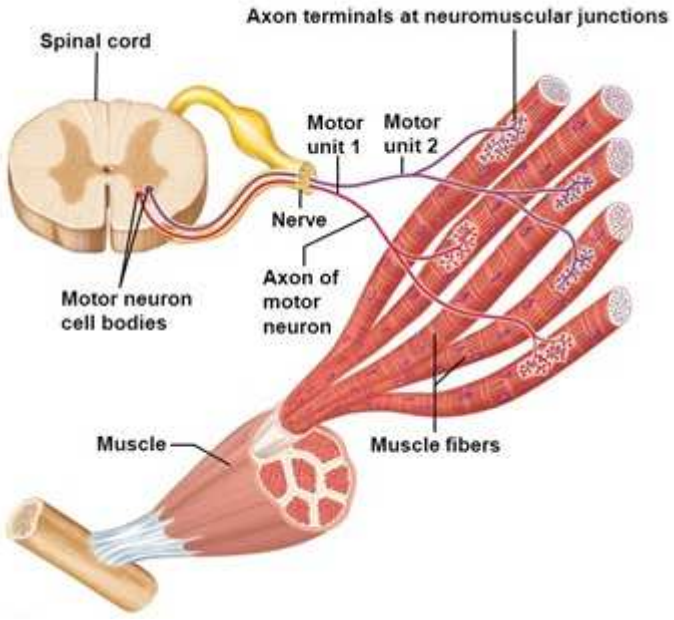

Figure 1.2 Schematic Representation of a Motor Unit [46].

well-trained physical therapist should be involved in data collection experiments which can be agonizing [48, 49]. Surface EMG is a non-invasive technique in which a pair or multiple electrodes are used for recording muscle activity from the skin above the target muscle. Due to its easy usage, surface electrodes are commonly used in research studies. Most of the important limb and trunk muscles can be measured by surface electrodes [45].

Unfiltered and unprocessed raw EMG signal's peak-to-peak amplitude range from 0 to 10 millivolts and the usable frequency range between 6 and 500 Hz. In addition to low amplitude, EMG signals can be easily deformed during recording because of external factors, such as skin tissue characterization, noise, and electrode movements [21]. Therefore, according to the application, EMG signals need to be processed. Noises generated by electronics equipment and sources of electromagnetic radiation can be one to three times greater than the raw signal. These artifacts can be eliminated by stop band filters at between 50 and 60 Hz. The interface between the surface electrodes and skin and the movement of the electrode cables are another main sources contributing to the motion artifact which can be eliminated by using low-pass filters [50]. After filtration, the signal is rectified to turn all the signal values

integrative. Lastly, to create a linear envelope in the signal in order to evaluate and process the signal easily, the signal is smoothed [51]. The whole process is shown in Figure 1.3.

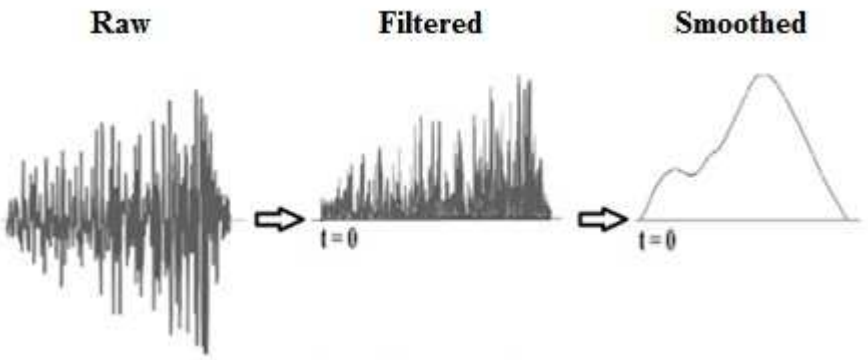

Figure 1.3 EMG Signal Processing [52].

1.3 Neural Networks

Artificial neural networks are mathematical models that mimic aspects of the biological nervous system's operating structure. To understand the artificial neural network, it is a necessity to become familiar with the general properties of the biological neural system [53].

The fundamental unit of the nervous system is the neuron, which has (1) a nucleus with simple processing abilities, (2) backward extensions called dendrites and (3) a forward extension called axon [54]. Dendrites are cellular projections whose primary function is to receive the synaptic signals (electrochemical stimulation) received from adjacent cells and transmit them to the nucleus that is in the soma (cell body). The axon is a transmission line, which transfers the output, generated in soma according to incoming stimulations, to adjacent cells [54]. The output of each neuron is determined in the nucleus by cellular assessment of received stimulations. If the total excitation exceeds a threshold value, an action potential is generated to stimulate adjacent neuron, muscle or gland. Thus, the information is transmitted from one neuron to another [14].

As in biological neural network, basic building block of every artificial neural network is the artificial neuron, which is a simple mathematical function conceived as a model of biological neurons. Such a model has three layers as shown in Figure 1.4: (1) *multiplication layer* is in which the inputs of network are weighted by being multiplied by their individual weight at the entrance; (2) *summation layer* is in which previously weighted inputs and bias are summed; (3) *activation layer* is in which output of the sum function is passed through a transfer function, that determines the functional behavior of the neuron [55].

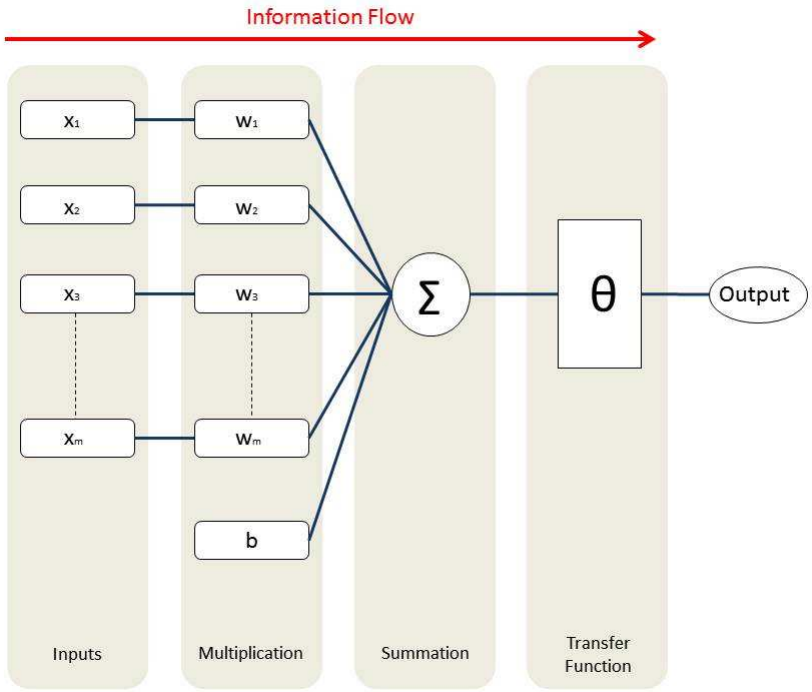

Figure 1.4 Graphical representation of a simple artificial neuron (perception).

Artificial neuron given in Figure 1.4 has m number of *input signals* (x_1 through x_m) and *weights* assigned to these inputs (w_1 through w_m). Also, one input called *bias* (b) with a constant value (typically +1 or -1) is given to improve properties of the neuron.

Mathematical representation of the artificial neuron output is

$$y = \theta \cdot \sum_{j=1}^{m} (x_j w_j + b) \tag{1.1}$$

where θ is the transfer function of the neuron and y is the neural network output.

Even though one single artificial neuron is a simple structure in terms of its working principle and capabilities, an artificial neural network constructed by interconnected artificial neurons becomes a powerful tool for applications where the complexity of the data or task makes the design a model or function by hand impracticable like in robotics applications, including directing manipulators and prosthesis [55, 56].

In Figure 1.5, commonly used **multilayer feed-forward neural network** is shown. This neural network structure is called multilayer feed-forward; because (1) it has a layer of processing (i.e., the hidden layer) in addition to the input and output layer, and (2) output of each neuron from one layer is fed into the inputs of each neuron in the following layer [57]. Typically, all neurons in a layer are connected with all neurons at the next layer while ones in the same layer are not interconnected [58].

Neural network shown in Figure 1.5 has three inputs (x_1, x_2 and x_3) and one output (y). There are three neurons in input layer, two neurons in hidden layer and one neuron in output layer. Weights for each interconnection, biases and transfer functions for each neuron are given as w, b and θ, respectively. Analytical description of this neural network is given in sets of equations Eq. 1.2, 1.3, 1.4 and 1.5.

Outputs of each neuron in input layer are;

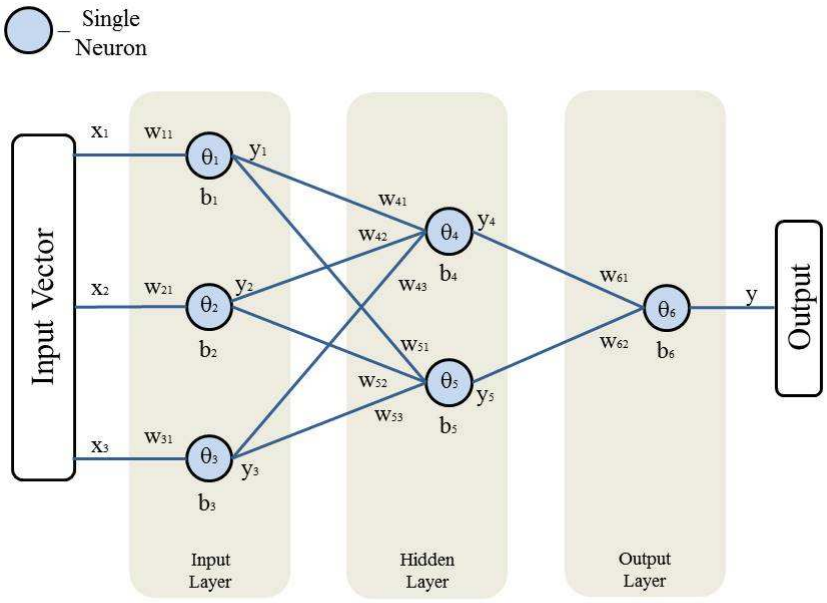

Figure 1.5 Example of a simple multilayer feed-forward artificial neural network with one hidden layer.

$$\begin{aligned} y_1 &= \theta_1 \cdot (x_1 w_{11} + b_1) \\ y_2 &= \theta_2 \cdot (x_2 w_{21} + b_2) \\ y_3 &= \theta_3 \cdot (x_3 w_{31} + b_3) \end{aligned} \tag{1.2}$$

Outputs of each neuron in hidden layer are;

$$\begin{aligned} y_4 &= \theta_4 \cdot (y_1 w_{41} + y_2 w_{42} + y_3 w_{43} + b_4) \\ y_5 &= \theta_5 \cdot (y_1 w_{51} + y_2 w_{52} + y_3 w_{53} + b_5) \end{aligned} \tag{1.3}$$

Output of the neuron in output layer is;

$$y = \theta_6 \cdot (y_4 w_{61} + y_5 w_{62} + b_6) \tag{1.4}$$

Final form of the neural network output based on network inputs and properties of each neuron in network is;

$$\begin{aligned} y = \theta_6 \cdot \Bigg(& \theta_4 \cdot \Big(\theta_1 \cdot (x_1 w_{11} + b_1) \cdot w_{41} + \theta_2 \cdot (x_2 w_{21} + b_2) \cdot w_{42} + \\ & \theta_3 \cdot (x_3 w_{31} + b_3) \cdot w_{43} + b_4 \Big) \cdot w_{61} + \\ & \theta_5 \cdot \Big(\theta_1 \cdot (x_1 w_{11} + b_1) \cdot w_{51} + \theta_2 \cdot (x_2 w_{21} + b_2) \cdot w_{52} + \\ & \theta_3 \cdot (x_3 w_{31} + b_3) \cdot w_{53} + b_5 \Big) \cdot w_{62} + b_6 \Bigg) \end{aligned} \tag{1.5}$$

Analytical description of such a simple feed-forward neural network shows that optimizing the artificial neural networks' parameters by hand is impractical. Therefore, a variety of learning techniques for multilayer networks are developed while the most popular one is a supervised learning paradigm called the back-propagation algorithm, [59, 60]. Parameters of the neural network are determined and set by using training datasets consisting inputs and desired outputs [61].

The back-propagation algorithm repeats a two-phase cycle: (1) propagation and (2) weight update [62]. When the input of the training set is presented to the network whose neuron weights are initially randomized, it is propagated forward through the network until it reaches the output layer. Then, the output is compared with the target output using an error function to calculate errors for each neuron in every layer. The result of the error function is back-propagated from the output layer until the input layer and the algorithm adjusts the weights of each connection in order to reduce the errors. After repeating this process for a sufficiently large number of training cycles

(iterations), the network is converged to a state where the error of the calculations is very small [63].

2. METHOD

2.1 Datasets For Development of the Neural Networks

In order to develop, train and test the targeted neural networks, datasets that consist of EMG signals, ground reaction forces in three axes (anterior-posterior (F_x), medial-lateral (F_y) and vertical (F_z) direction) and position and moment change of the ankle joint recorded during gait, were needed. A study with a similar protocol to the present work, that shares needed data for public use was used for that purpose [64]. Below the approaches of Ferrarin et al., [64] are summarized:

Forty able-bodied subjects participated in that study, were classified into two age groups:

Adult group: 20 (9 males, 11 females) participants were included (ages vary from 22 to 72 years; mean 43.1 ± 15.4; body mass 68.5 ± 15.8 kg; height 1.71 ± 0.10 m).

Young group: 20 (9 males, 11 females) participants were included (ages vary from 6 to 17 years; mean 10.8 ± 3.2; body mass 41.4 ± 15.5 kg; height 1.47 ± 0.20 m).

Surface EMG signals were registered from the tibialis anterior (TA), soleus (SOL), gastrocnemius medialis (GAM), peroneus longus (PL), rectus femoris (RF), vastus medialis (VM), biceps femoris (BF) and gluteus maximus (GM) muscles using **an 8-channel wireless electromyography, ZeroWire (Aurion, Milano, Italy)**. Using **a 9 cameras SMART-E motion capture system (BTS, Milano, Italy)**, 3D kinematics were measured at 60 Hz. While retroreflective markers were positioned on the head, upper limbs, trunk, pelvis and lower limbs. Ground reaction forces (GRFs) were recorded from **two force plates (Kistler, Winterthur, Switzerland)**, at 960 Hz sampling frequency. 3D kinematics, dynamics, and EMG were considered if complete data were available over at least one stride.

Records were classified according to the gait speeds. (1) *Natural speed* class includes records from the trials in which the subjects were instructed to walk at their natural speed. Walking trials recorded at a later stage when subjects were asked to perform progressively increasing or decreasing their speed, were further classified based on walking speed normalized to subject's height (v/h [%BH s^{-1}]):
(2) *Very slow speed class* for (v/h) < 0.6 s^{-1};
(3) *Slow speed class* for 0.6 %BH $s^{-1} \leq$ (v/h) $<$ 0.8 %BH s^{-1};
(4) *Medium speed class* for 0.8 %BH $s^{-1} \leq$ (v/h) $<$ 1 %BH s^{-1};
(5) *Fast speed class* for (v/h) $\geq$ 1 %BH s^{-1}.

Thus, for each of the 40 subjects, five datasets (one for each walking class) considered include EMG signals, ground reaction forces, ankle position and moment change over a gait cycle. Therefore, two hundred datasets were produced in total. However, the authors concluded that such high number of datasets was hard to handle. Therefore, for each age group, five averaged datasets for five walking classes were calculated. Consequently, in their database shared, 10 averaged datasets were offered by Ferrarin et al [64].

Simultaneously recorded GRFs and joint moments were normalized to body mass. EMG signals were treated using rectification and low pass filtering using 5th order Butterworth with 3 Hz cut-off frequency. To allow inter-subject and inter-task comparisons, EMG signals were subjected to intra-subject normalization similarly to peak dynamic method.

2.2 Training Of The Developed Neural Networks

In the present work, the networks were trained in MATLAB by using Bayesian regularization back-propagation, which is a network training algorithm that updates the weight and bias values according to Levenberg-Marquardt optimization. It minimizes a linear combination of squared errors and weights and then determines the correct combination so as to produce a network that generalizes well [65].

Two neural networks to estimates position and moment change in the ankle separately were constructed for each type of neural network structure, and these were trained by the training datasets that generated according to the neural network's input-output combination. From the database by Ferrari et al. [64], datasets from *very slow*, *slow*, *medium* and *fast speed classes* of both young and adult age group were selected as training datasets. Inputs of these were averaged EMG signals of eight muscles and averaged GRFs in three axes, outputs were averaged moment and position changes in the ankle during a gait cycle. Thus, a total of 8 datasets, referred to as *averaged inputs*, could be used for network training.

To prevent inadequate network training that could occur due to the limited amount of data sets, a training protocol was proposed. Via this protocol, new datasets were generated by manipulating the averaged inputs over their standard deviations given in the database. Minimum and maximum standard deviations of each data referred to as the *minimum limit input* and the *maximum limit input*, respectively.

To generate new training datasets, a script was written in MATLAB. This script helped to create randomized inputs between the minimum and maximum limit inputs, as shown in Figure 2.1 and 2.2. By doing this for each input (EMGs and GRFs) in a dataset, **a randomized input dataset** was generated, and consequently, the number of training datasets increased from 8 to 32 in total by a set of **randomized input datasets** (four new datasets from each training datasets). It was hoped that this protocol would improve the network training efficiency by increasing the possible input combinations.

2.3 Proposed Neural Networks

The proposed algorithm is desired to work with minimum error and stability without requiring an extra mathematical model or process to smooth and improve the output. Also, since EMG sensors are easily affected by external factors and redundancy of these cause user's discomfort, the development of a system that requires a few of

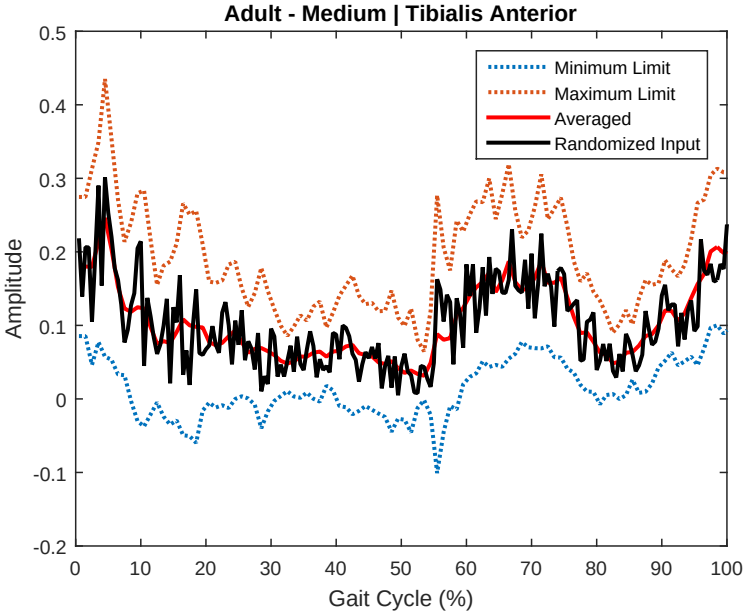

Figure 2.1 EMG amplitude of the TA from a randomized input. The red dashed line shows the maximum limit input of TA's normalized EMG amplitude from adult age group recorded during medium speed walking, while blue dashed line shows the minimum limit input. On the other hand, the red solid line shows the averaged input and black solid line shows the generated dataset, which is randomized around averaged data within the minimum and maximum limit inputs.

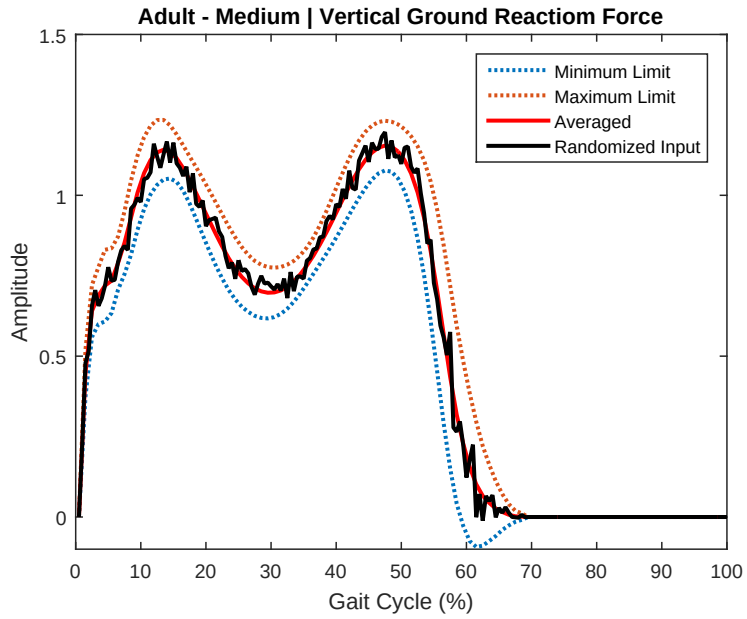

Figure 2.2 Normalized ground reaction force amplitude in vertical direction from a randomized input. The red dashed line shows the maximum limit input of normalized vertical ground reaction force from adult age group recorded during medium speed walking while blue dashed line shows the minimum limit input. On the other hand, the red solid line shows the averaged input and the black solid line shows the generated dataset, which is randomized around averaged data within the minimum and maximum standard limit.

these sensors as possible is important for both system reliability and user comfort. Therefore, it is aimed to design the most effective neural network structure using the minimum number of EMG as network inputs.

Three neural network structures, which are different from each other in terms of the number of muscle inputs, developed for these purposes: **TYPE I**, consisting 6 muscles' activation signals as network inputs; **TYPE II**, consisting 5 muscles' activation signals as network inputs; and **TYPE III**, consisting 3 muscles'activation signals as network inputs.

First, to evaluate the training protocol effectiveness in neural network estimation, two **TYPE I** neural network structures have been developed:
(1) **TYPE $\mathbf{I_{TP-}}$** and
(2) **TYPE $\mathbf{I_{TP+}}$**.

Unlike TYPE I_{TP-}, TYPE I_{TP+} neural networks were trained according to the proposed protocol. Since walking is a complicated task where the ankle, knee and hip joints work in a harmony with each other, inputs of TYPE I were determined to include EMG signals from main 6 lower leg muscles measured for completeness: (1) Tibialis Anterior, the dorsiflexor of the ankle. (2) Gastrocnemius Medialis and (3) Soleus, plantar flexors of the ankle. (4) Rectus Femoris, the extensor of the knee. (5) Biceps Femoris, the flexor of the knee and (6) Gluteus Maximus, the extensor of the hip.

The comparison between the two TYPE I neural networks' results demonstrated that the proposed training protocol provided a significant improvement in position estimation such that the averaged correlation coefficient was increased from to 69.79% $\pm$7.26 to 98.70% $\pm$0.67. Therefore, **neural networks developed in later stages were trained with the proposed protocol**.

TYPE I_{TP+} neural network estimation results showed high correlations with the targets and total errors were in the acceptable range. Accordingly, these results were

considered as references for the evaluation of other neural networks to be developed, and it was aimed to build an efficient one using fewer EMG network inputs.

As it is in TYPE I, the inputs of **TYPE $\mathbf{II_{GRF-}}$** neural network were also determined to include only EMG signals from muscles that are responsible for the three main joints movements. However, the EMG signal from the soleus muscle was excluded to test if a neural network structure with a less EMG inputs may be sufficient for the intended objective. The reason for the selection of soleus muscle is depending on the level of the amputation, it may not be possible to collect an accurate EMG signal from it.

TYPE II_{GRF-} neural network results also showed high correlation with the targets as in TYPE I_{TP+}, but errors in moment and position estimations were increased. Nevertheless, the promising high correlation results were motivated for the development of a network whose inputs are EMG signals obtained only from the muscles under the knee.

Since dorsiflexors and plantar flexors are the main lower leg muscles that act on the ankle, inputs of **TYPE $\mathbf{III_{GRF-}}$** were determined to include EMG signals from only below-knee muscles: (1) Tibialis Anterior, (2) Soleus and (3) Gastrocnemius Medialis muscles. TYPE III_{GRF-} did not show such a high correlation like others, and also the averaged total error has been considerably increased.

As natural walking, ankle angle and moment changes vary due to the characteristics of the ground such as friction or slope. Therefore, adding ground reaction forces as inputs of a neural network were known to affect moment and position estimation positively [8,9,19,20]. Consequently, in the development of the **TYPE $\mathbf{III_{GRF+}}$** neural network, in addition to the EMG signals from the specified muscles in TYPE III_{GRF-} neural network, the ground reaction forces in 3 axes were also used as inputs. This network was developed to measure and demonstrate the effectiveness of the ground reaction forces. In addition, it was wanted to test if a network whose inputs are EMG signals from the below-knee muscles and ground reaction forces fulfills the expectations.

The proposed neural networks had time delay feed-forward multilayer neural network architecture, which was a feed-forward network consisting of three layers: an **input layer** and one **hidden layer** with delays followed by an **output layer**. Time delay neural networks (TDNN) works on sequential inputs which makes the network generate an output based on time-varying inputs. As an example, a neuron from the hidden layer with N data time delay is given in Figure 2.3. It has one input signal (x), one weight (w) assigned to this input and one output.

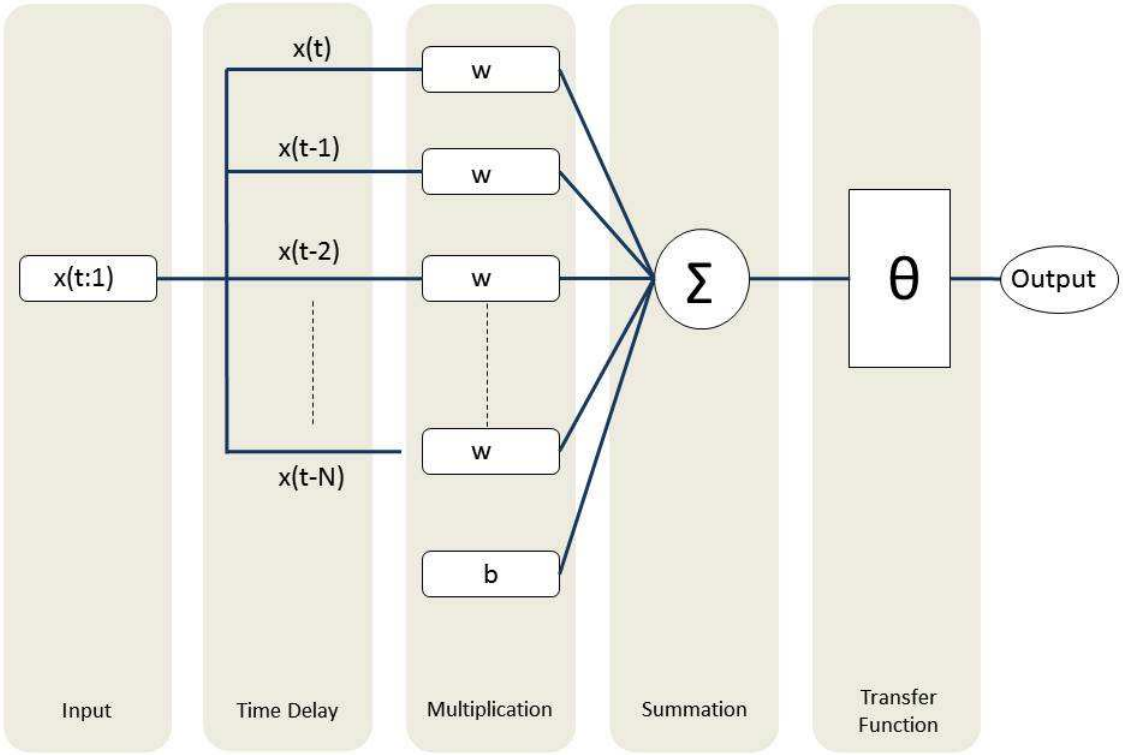

Figure 2.3 Representation of a simple neuron with time delay.

Mathematical representation of the neuron output is

$$y = \theta \cdot \big(x(t)w, x(t-1)w, x(t-2)w, ..., x(t-N) \big) \tag{2.1}$$

where θ is the transfer function of the neuron and y is the neural network output.

The proposed networks had 32 neurons with a nineteen-data-tapped delay in the

hidden layers. These values were chosen on the basis of previous works and experience obtained as a result of experiments [14,66]. While the number of neurons in the input layer varies according to the neural network type (TYPE I - III), for each neural network type, two neural networks with a single output were developed. One of which predicted the ankle position and the other of which predicted the ankle moment.

For every neural network, a sigmoidal transfer function was used between in the hidden layer, because the sigmoidal function is bounded differentiable real function that is defined for all real input values and has a positive derivative at each point. In the output layer, a linear transfer function was used so that the neural outputs could take on any value. The sigmoidal and linear transfer functions were *tansig* and *purelin* functions from the neural network toolbox of MATLAB as shown in Figure 2.4.

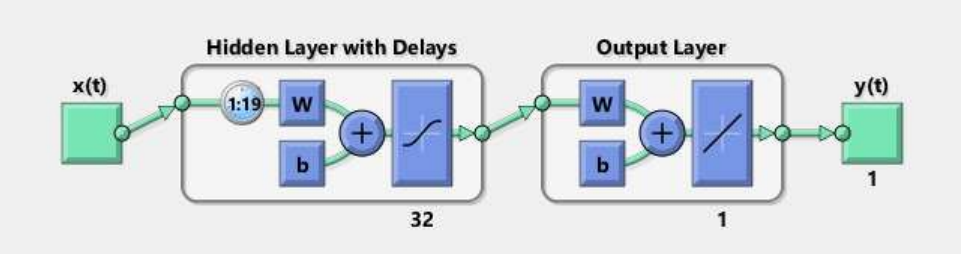

Figure 2.4 Basic representation of one of the proposed neural networks.

2.4 Evaluation Of Neural Networks

Evaluation of the proposed neural networks' performance was planned to carry out with datasets from natural speed class of young and adult age group which were not used in training. However, considering that two datasets in total would not be sufficient for evaluation of neural networks' performance, a set of new datasets listed below was produced from natural gait speed datasets by changing the EMG amplitudes of TA and GAM muscles. These muscles were selected because they are the major components of the ankle movement. Also, their sizes may be variable for each below-knee amputees so that inter-patient differences in the EMG amplitudes may occur.

- **Increased EMG Amplitude of TA**: TA's amplitudes from natural speed gait datasets of both age groups were increased by fifteen percent of standard deviation range(Figure 2.5).
- **Increased EMG Amplitude of GAM**: GAM's amplitudes from natural speed gait datasets of both age groups were increased by fifteen percent of standard deviation range.
- **Decreased EMG Amplitude of TA**: TA's amplitudes from natural speed gait datasets of both age groups were decreased by fifteen percent of standard deviation range (Figure 2.6).
- **Decreased EMG Amplitude of GAM**: GAM's amplitudes from natural speed gait datasets of both age groups were decreased by fifteen percent of standard deviation range.
- **Increased EMG Amplitude of TA & GAM**: TA and GAM's amplitudes from natural speed gait datasets of both age groups were increased by ten percent of standard deviation range.
- **Decreased EMG Amplitude of TA & GAM**: TA and GAM's amplitudes from natural speed gait datasets of both age groups were decreased by ten percent of standard deviation range.

The test datasets that listed above not only increased the verification accuracy in neural network evaluation but also enabled to test the flexibility of networks against changed muscle activities. The choices of amplitudes of increases or decreases implemented rely on the previous work done by Sepulveda et al [14].

In order to evaluate the performances of neural networks and make a comparison among them, a real-time ankle position and moment estimator script was written in which each neural network type was tested. The following three statistical assessments were conducted in order to determine whether the networks have been successfully trained or not: (1) **Root mean square error method**, which is used for calculating

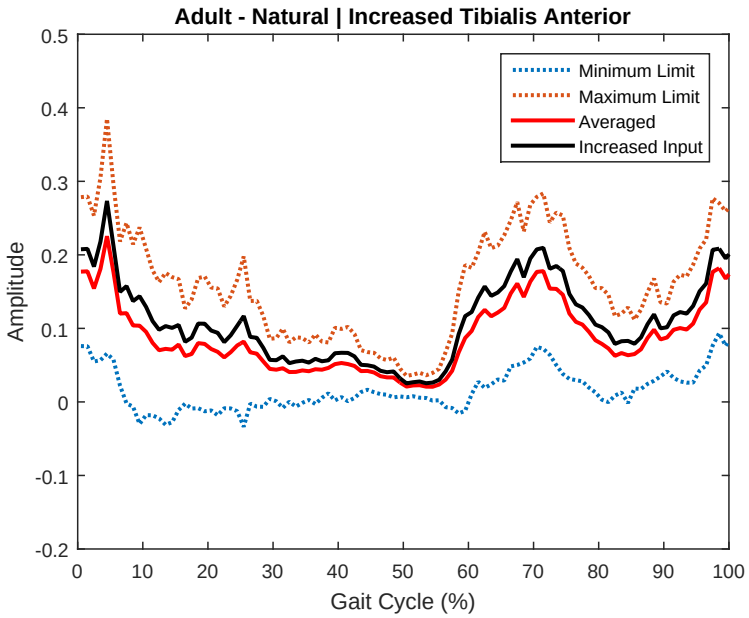

Figure 2.5 Normalized EMG Amplitude of Tibialis Anterior Muscle from the "Increased EMG Amplitude of TA". The red dashed line shows the maximum limit input of TA's normalized EMG amplitude from adult age group recorded during natural speed walking, while blue dashed line shows the minimum limit input. On the other hand, the red solid line shows the averaged input and black solid line shows the derived input.

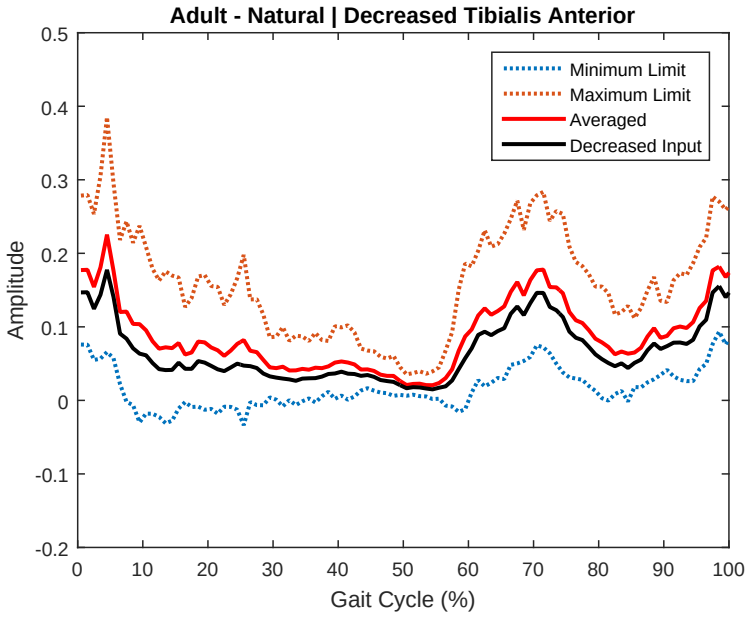

Figure 2.6 Normalized EMG Amplitude of Tibialis Anterior Muscle from the "Decreased EMG Amplitude of TA". The red dashed line shows the maximum limit input of TA's normalized EMG amplitude from adult age group recorded during natural speed walking, while blue dashed line shows the minimum limit input. On the other hand, the red solid line shows the averaged input and black solid line shows the derived input.

the difference between the output signal of the network and the target signal. (2) **Pearson's correlation coefficient**, which is a measure of the linear correlation (dependence) between the output and the target signal. (3) **Total error**, which is the summation of absolute errors. The overall evaluation of each neural network type was made by taking the average of the statistical results obtained from each test datasets (averaged correlation coefficient, averaged RMSE and averaged total error).

Real-time position and moment estimates can follow the target in an unstable manner by fluctuations, and since the total error is the sum of the absolute errors between the expected and the network result, it gives a clear understanding of the system's stability. This caused network structures that are different from each other by their errors despite their correlation values are high. An unstable structure may cause users to lose balance during walking or walk unnaturally because the output of the planned algorithm is given directly to the actuators of the mechanical system without any additional regulation or verification. Therefore, the criterion for the success or failure of the network structure's output is not only the correlation coefficient between the expected but also the sum of errors.

3. RESULTS

In this section, the position and moment estimation results for each type of developed neural network structures are shown and detailed. Networks were tested with test datasets consisted of natural classes of both age groups and ones that were generated from these classes by changing their TA and GAM muscles' amplitudes. Statistical results that were calculated based on the expected and obtained results for the developed network structures are given. The results of these statistical data are presented graphically on the response of each neural network when the dataset of natural speed class of young age group is given as input. The reason for choosing this dataset is that this is the best representation of the averaged total error, RMSE value and correlation coefficient for each network type. For each network structure, results obtained with other datasets are presented in the APPENDIX section.

During the training of TYPE I_{TP-} neural networks, only training datasets have been used while for other types, within the scope of the proposed training protocol, randomized input datasets were used. Therefore, in order to evaluate the effectiveness of the proposed training protocol, TYPE I_{TP+} neural networks with the same structure as TYPE I_{TP-} were developed.

For the TYPE I_{TP-} networks, the averaged correlation coefficient between the position estimation result and the target position could not exceed 69.76% $\pm$7.26. On the contrary, the averaged correlation coefficient of TYPE I_{TP+} which was tested with the same datasets was calculated as 98.70% $\pm$0.67 (Figure 3.1).

Below, the estimation results are presented in figures, which include four panels each: The panels in the first-row show real-time position estimation results of the related neural network structures compared to the expected response, while panels in the second row show the absolute values of the errors.

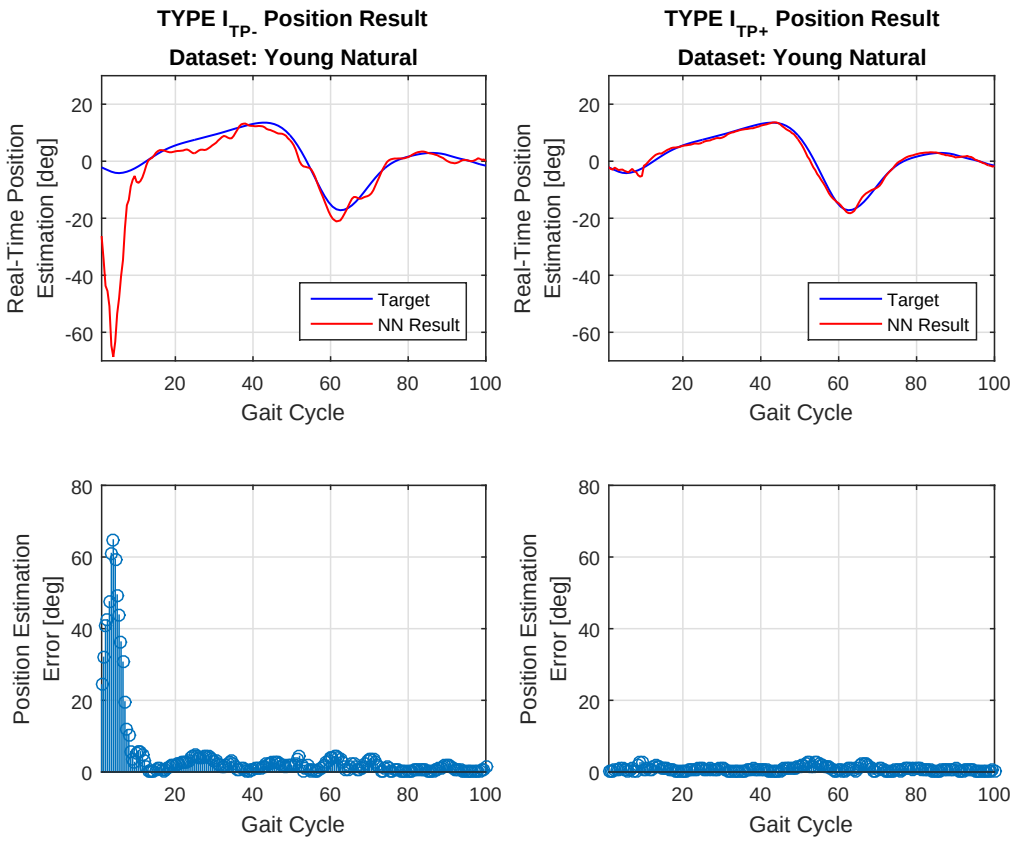

Figure 3.1 Position estimation results of TYPE I_{TP-} and TYPE I_{TP+} when the natural speed class dataset from young age group is given as input. TYPE I_{TP-} failed to make a correct estimation for all along the gait. Due to its design, large errors were observed in first 10% of the gait. For the rest, the network continued to run irregularly, resulting in erroneous results. On the contrary, TYPE I_{TP+} produced steady and accurate position estimation.

TYPE I_{TP-} and TYPE I_{TP+} results demonstrated the effectiveness of the proposed training protocol. It has significantly improved the correlation coefficient and reduced the errors in position estimation. The averaged RMSE and total error in position estimation for TYPE I_{TP-} neural network have been 10.40 $\pm$1.56 and 894.03 $\pm$197.47 degrees. When TYPE I_{TP+} results were examined, the averaged RMSE and total error values were observed to decrease to 1.44 $\pm$0.35 and 229.59 $\pm$58.87 degrees. In addition, the averaged correlation coefficients were increased from 69.76% $\pm$7.26 to 98.70% $\pm$0.67.

Moment estimator networks of both TYPE I neural networks demonstrated

high correlation coefficient result. The averaged correlation coefficients of TYPE I_{TP-} and TYPE I_{TP+} neural networks were calculated as 96.86% ±1.08 and 99.47% ±0.42, respectively (Figure 3.2). Although the correlation values were high for both, when the total error and RMSE values were examined, the results of TYPE I_{TP+} showed the improving effect of the training protocol. In tests of TYPE I_{TP-}, RMSE and total error were calculated as 0.131 ±0.02 and 15.92 ±4.19 Nm/kg. However, as a result of the improvements in the first 10 percent of the gait, the averaged RMSE and total error values were decreased to 0.053 ±0.02 and 6.54 ±2.33 Nm/kg in TYPE I_{TP+}.

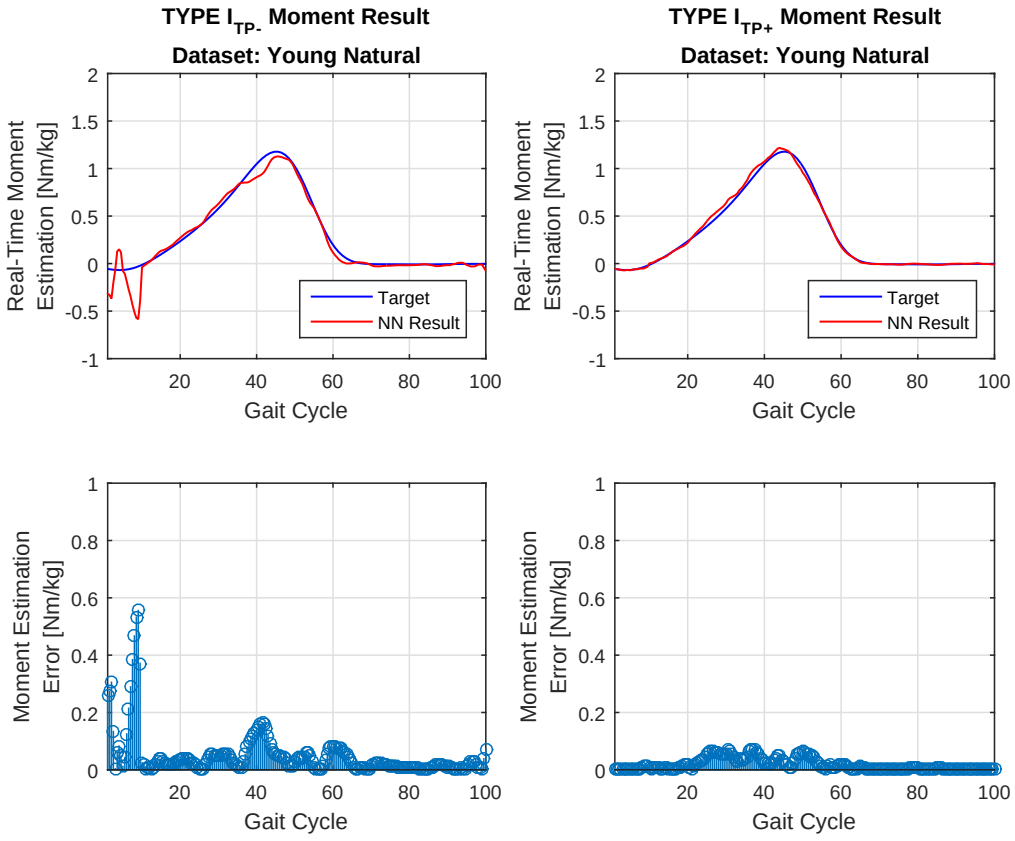

Figure 3.2 Moment estimation results of TYPE I_{TP-} and TYPE I_{TP+} when the natural speed class dataset from young age group is given as input. As in position estimation, TYPE I_{TP-} failed to make a steady moment estimation. Due to its design, large errors were observed in first 10% of the gait. Contrary to TYPE I_{TP-}, TYPE I_{TP+} has produced a result with high accuracy for every stage of gait.

On the basis of position and moment estimation results, the proposed training protocol was decided to be used for the training of the neural networks to be developed during the studies to reduce the number of muscles inputs.

TYPE II_{GRF-} and TYPE III_{GRF-} neural networks have been designed and developed to test the possibility of an active ankle prosthesis development that requires less EMG sensors as system inputs. Considering the possibility that it may not be possible to collect an accurate EMG signal from the soleus muscle due to the level of amputation, TYPE II_{GRF-} neural network structure, in which the EMG signal of soleus muscle was not used as an input, has been built. On the contrary, for the situations where a quality signal can be collected from the soleus via surface EMG sensors, TYPE III_{GRF-} networks have been developed where only EMG signals from the below-knee muscles were used as the network inputs. Evaluation of these two network structures was carried out based on the results obtained from TYPE I_{TP+} results.

The averaged correlation coefficient, RMSE, and total error values obtained during the position estimation of TYPE I_{TP+}, TYPE II_{GRF-} and TYPE III_{GRF-} are tabulated in Table 3.1.

Table 3.1
Position estimation results of TYPE I_{TP+}, TYPE II_{GRF-} and TYPE III_{GRF-} obtained from test datasets.

	Averaged RMSE [deg]	Averaged Total Error [deg]	Averaged Correlation Coefficient [%]
TYPE I_{TP+}	1.44 ±0.35	229.59 ±58.87	98.70 ±0.67
TYPE II_{GRF-}	1.68 ±0.46	257.17 ±68.09	98.56 ±0.73
TYPE III_{GRF-}	5.94 ±0.99	815.92 ±132.84	60.00 ±25.38

When the position estimation results for these network structures are compared, excluding the EMG signal of the soleus muscle from the network inputs did not make a significant alteration in the averaged correlation coefficient and errors. But using the EMG signals from only the below-knee muscles did not only make a huge increase in errors but also an enormous decrease in the averaged correlation coefficient. Similar results were also obtained during moment estimation (Table 3.2).

Estimation results of TYPE I_{TP+}, TYPE II_{GRF-} and TYPE III_{GRF-} obtained with the natural speed class dataset from young age group are presented in Figure 3.3,

Table 3.2
Moment estimation results of TYPE I_{TP+}, TYPE II_{GRF-} and TYPE III_{GRF-} obtained from test datasets.

	Averaged RMSE [Nm/kg]	Averaged Total Error [Nm/kg]	Averaged Correlation Coefficient [%]
TYPE I_{TP+}	0.053 ±0.02	6.54 ±2.33	99.47 ±0.42
TYPE II_{GRF-}	0.077 ±0.03	10.10 ±4.39	99.02 ±0.72
TYPE III_{GRF-}	0.125 ±0.03	16.71 ±3.53	95.88 ±1.98

3.4 and 3.5. Below, the estimation results are presented in figures, which include four panels each: The panel on the upper left shows the position estimation result of the related neural network structure compared to the expected response, while the upper right panel shows the moment estimation result in a similar way. Panels on the second row show the absolute values of the errors in the position and moment estimation.

When the results were analyzed, it was determined that the minimum amount of EMG signal requirements for a neural network without a force and/or torque feedback, is five. Also, these muscles, whose EMG's are in use, should be the main actuators of three joints (the hip, the knee, and the ankle) that work in harmony during the walking.

Since it is known that using the torque and/or force feedback as an algorithm input improves the output [8, 9, 19, 20], it was wanted to test the network response whose inputs are EMG signals from tibialis anterior, soleus and gastrocnemius medialis muscles and ground reaction forces in three axes. For this purpose, TYPE III_{GRF+} neural networks were developed.

To make a performance comparison, the position (Tables 3.3) and moment (Tables 3.4) estimation results of all the proposed network structures are tabulated.

The results obtained from TYPE III_{GRF+} with the natural speed class dataset from young age group that was used to compare network performances in the previous

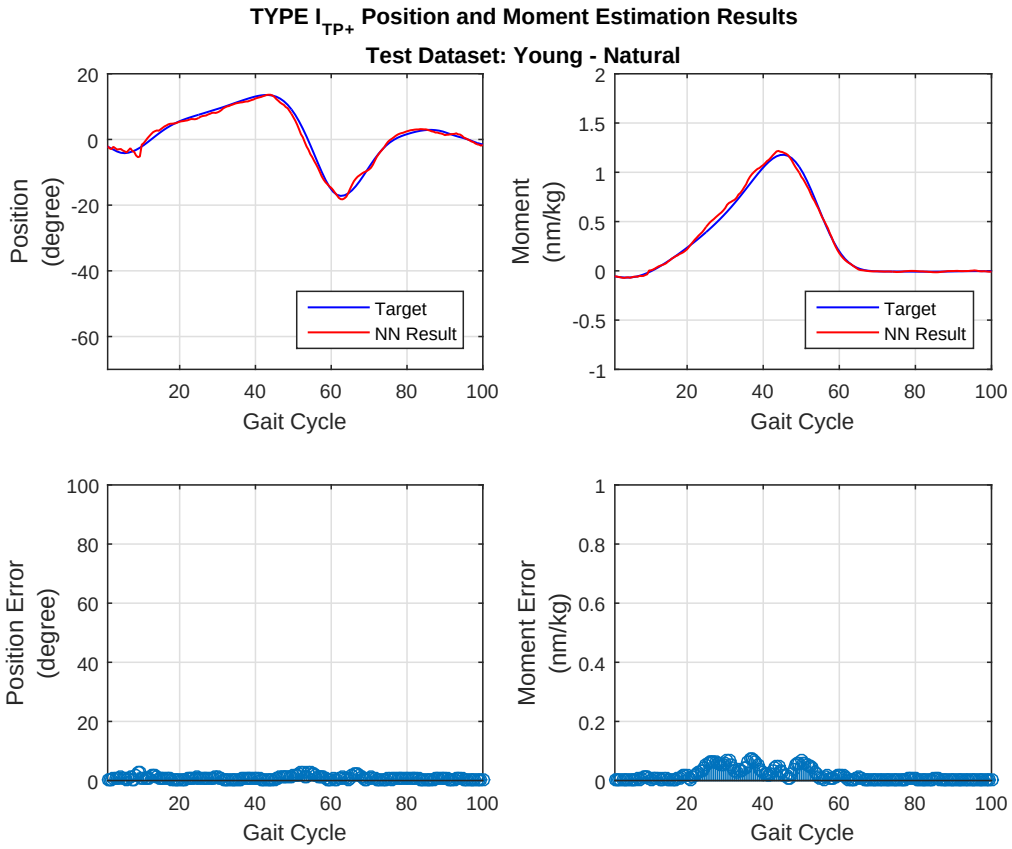

Figure 3.3 TYPE I_{TP+} neural networks' position and moment estimation results when the natural speed class dataset from young age group is given as system input. Total errors calculated during the position and moment estimations are 154.23 degrees and 3.51 Nm/kg while correlation coefficients are 99.24% and 99.81%, respectively.

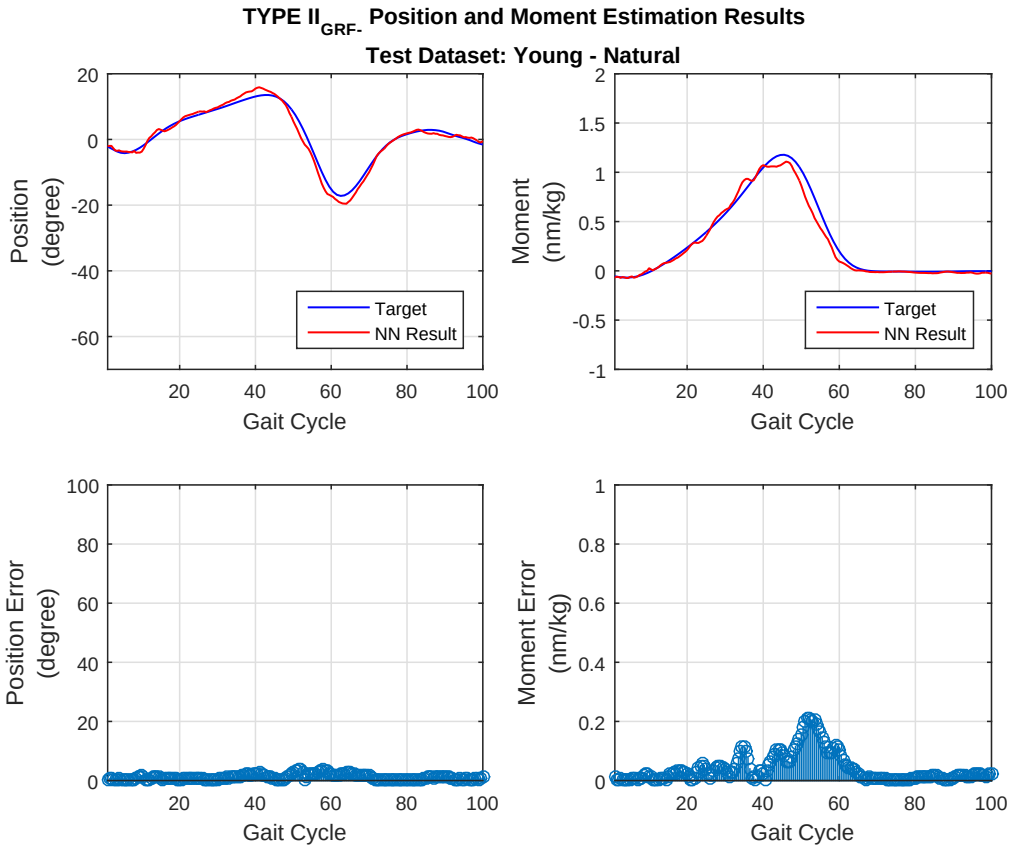

Figure 3.4 TYPE II_{GRF-} neural networks' position and moment estimation results when the natural speed class dataset from young age group is given as system input. Total errors calculated during the position and moment estimations were 218.24 degrees and 8.01 Nm/kg while correlation coefficients were 99.19% and 99.01%, respectively.

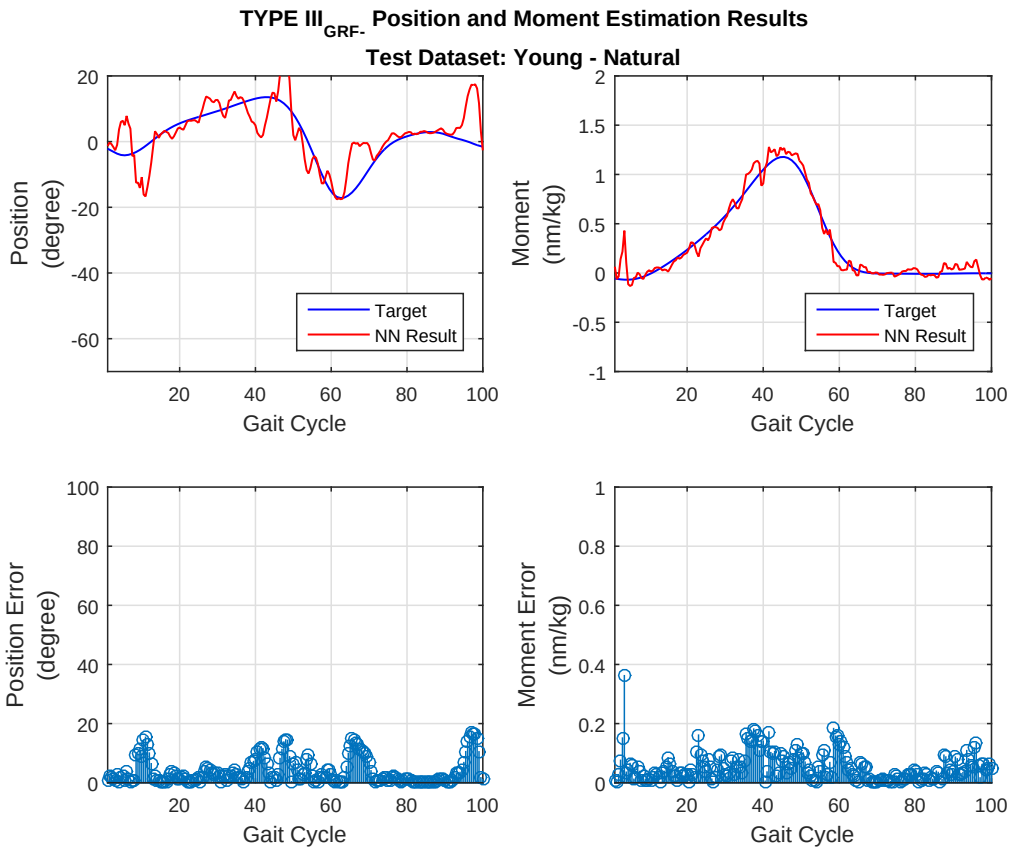

Figure 3.5 TYPE $\text{III}_{\text{GRF}-}$ neural networks' position and moment estimation results when the natural speed class dataset from young age group is given as system input. Total errors calculated during the position and moment estimations were 786.63 degrees and 10.64 Nm/kg while correlation coefficients were 72.36% and 98.25%, respectively. Comparing with the TYPE $\text{I}_{\text{TP}+}$ results errors in position were increased to 5.10 times while moment estimation total errors were increased to around 3 times. For position estimation the correlation coefficient decreased to 72.36% from 99.24% and RMSE value is increased to 5.97 degrees from 0.98 degrees.

Table 3.3
Position estimation results obtained using the test datasets.

	Averaged RMSE [deg]	Averaged Total Error [deg]	Averaged Correlation Coefficient [%]
TYPE I_{TP-}	10.40 ±1.56	894.03 ±197.47	69.76 ±7.26
TYPE I_{TP+}	1.44 ±0.35	229.59 ±58.87	98.70 ±0.67
TYPE II_{GRF-}	1.68 ±0.46	257.17 ±68.09	98.56 ±0.73
TYPE III_{GRF-}	5.94 ±0.99	815.92 ±132.84	60.00 ±25.38
TYPE III_{GRF+}	1.01 ±0.19	155.85 ±23.75	99.16 ±0.53

Table 3.4
Moment estimation results obtained using the test datasets.

	Averaged RMSE [Nm/kg]	Averaged Total Error [Nm/kg]	Averaged Correlation Coefficient [%]
TYPE I_{TP-}	0.131 ±0.02	15.92 ±4.19	96.86 ±1.08
TYPE I_{TP+}	0.053 ±0.02	6.54 ±2.33	99.47 ±0.42
TYPE II_{GRF-}	0.077 ±0.03	10.10 ±4.39	99.02 ±0.72
TYPE III_{GRF-}	0.125 ±0.03	16.71 ±3.53	95.88 ±1.98
TYPE III_{GRF+}	0.031 ±0.01	4.10 ±0.88	99.82 ±0.07

sections, are shown in Figure 3.6.

As expected, test results showed a better estimation for both the position and moment change in the ankle during a gait cycle with TYPE III_{GRF+} neural networks, compared to other networks. This shows that if the ground reaction forces are wanted to be used, collecting EMG signals from only the below-knee muscles are enough as system input. Otherwise, EMG signals from at least five muscles need to be collected.

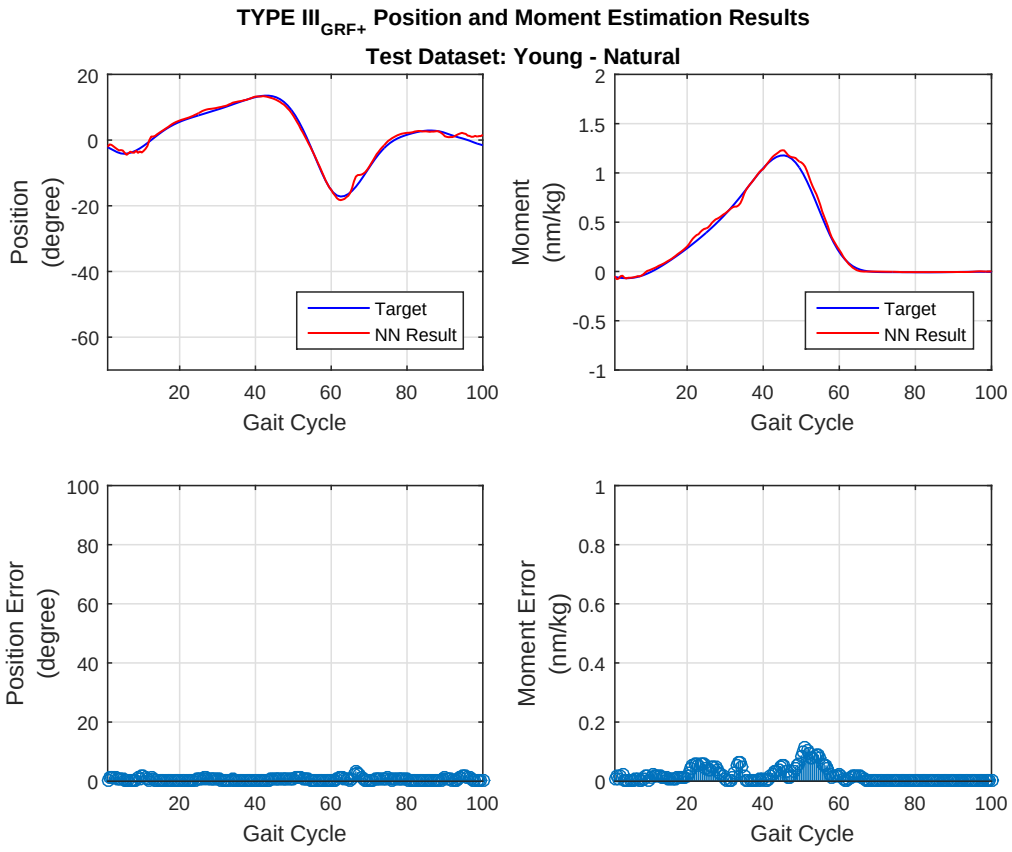

Figure 3.6 TYPE III_{GRF+} neural networks' position and moment estimation results when the natural speed class dataset from young age group is given as system input. Total errors during the position and moment estimations were 120.98 degrees and 3.85 Nm/kg while correlation coefficients were 99.44% and 99.81%, respectively. Comparing with the TYPE I_{TP+} results errors in position and moment estimation were decreased.

4. DISCUSSION

4.1 Selection Of A Neural Network Structure Based On The Sensor Infrastructure

The main objective of this study is to develop a neural network based algorithm for all kind of amputation levels, which makes real-time position and moments estimations of the ankle in a gait cycle and to find the minimum requirement of EMG signal inputs in such algorithms.

The first thing conducted within the present study was to increase the neural network training efficiency by proposing a neural network training protocol. Test results showed that neural networks trained without this protocol produced position estimation with enormous errors in the first ten percent of the gait cycle which corresponds to 20 data points. The reason for such a long-lasting large error is these networks have TDNN structure with nineteen data delays in the hidden layer. Since TDNN works with sequential inputs, an insufficient number of training datasets hinder the development of a neural network which produces the desired performance results at the beginning of the estimation. The proposed protocol allowed more accurate network training for this first ten percent of the gait cycle by increasing the number of the training dataset.

Three types of neural network different from each other in terms of the number of EMG inputs were developed. Prelusively, six muscles, which consist the extensor and the flexor muscles of the hip, knee and ankle joints, are selected as inputs for the TYPE I neural network structure. It has been observed that the neural networks in this structure estimate the target position and moment patterns with acceptable errors. Later, by excluding the soleus, the muscle input number was decreased to five and TYPE II neural networks were developed. Like TYPE I, the outputs of TYPE II were also satisfactory in terms of errors and correlation coefficient. However, when the number of EMG inputs is reduced to three, consisting signals collected from tib-

ialis anterior, soleus and gastrocnemius medialis muscles, the network outputs showed enormous errors and low correlation indicating that the desired pattern could not be followed.

Therefore, the test results show that an algorithm based on a neural network structure without any force and torque feedback requires the input of EMG signals from at least five of the muscles responsible for the movement of all of the hip, knee and ankle joints. However, if an algorithm is to be developed that uses only tibialis anterior, soleus and gastrocnemius medialis muscles' EMG signals as inputs, a force and/or torque feedback to the system will be needed. To do this, a mathematical model, which gives a continuous feedback to the main algorithm, can be developed [8,9,19,20]. Otherwise, as done in TYPE III_{GRF+}, ground reaction forces can be included into the neural network as inputs (Tables 3.3 and 3.4) in order to achieve sufficient success.

Sensors are widely used in robotic systems, especially in applications where there is human and machine interaction. However, contrary to general belief, the present study showed that the use of more sensors does not always lead to more accurate outputs or to the development of more stable systems. Therefore, the number of sensors should be optimized according to the application and needs of the system to be developed. Likewise, in the development of assistive robotic systems like active ankle prosthesis, using EMG signals as a continuous control command for prostheses may be problematic, because of their non-linear and non-stationary characteristic [67]. Also, considering that financial accessibility is one of the priorities in the development of such systems, the addition of any unnecessary item should be avoided. To avoid these kinds of problems, this study determined the requirement for a minimum number of EMG inputs for an algorithm, which makes the real-time estimation of the position and moment change in the ankle. Thereby, an ideal prosthetic system in terms of cost and usability can be developed by avoiding the unnecessary use of the EMG sensors.

Active ankle prosthesis' algorithm to be developed, based on the outcomes of this study, can gain flexibility according to system design, financial planning, and patient situation. If a force or torque sensor cannot be used because of the cost or

mechanical design difficulties, a minimum amount of EMG input requirement is five for a neural network based algorithm. This five EMG signals should also represent the movement of the three joints which work in harmony during the walking: the hip, knee and the ankle. On the contrary, if a force or/and torque feedback system can be used, three EMG inputs collected from tibialis anterior, soleus and gastrocnemius medialis muscles will be enough for a reliable prosthesis that functions properly. The algorithmic infrastructure may also be decided according to the amputation level of the patient. For patients from whom high-quality EMG signals cannot be collected from his/her lower leg muscles, a prosthesis which works with five EMG input can be recommended. In previous studies, different algorithmic infrastructures with modifiable inputs have been neither suggested nor developed in order to adapt the system to the patient according to his/her level of amputation [14, 68, 69].

In this study, a force feedback method was also tested. Unlike other studies, the proposed neural network structure is capable to provide high accuracy estimations with and without a force or torque feedback without a need of an extra mathematical model or a supportive neural network [17, 52, 70]. The ground reaction forces in three axes were fed into the algorithm as network inputs in addition to the EMG signals collected from tibialis anterior, soleus and gastrocnemius medialis muscles, and results were assessed. This showed that this type of network structure produces more stable behavior in outputs and improved estimation results (Tables 3.3 and 3.4). Therefore, the positive effect of a force feedback is once again observed, and it is demonstrated that since a neural network based algorithm fulfills the needs of active ankle prosthesis, force feedback can be implemented in the algorithm by using the sensor outputs as network inputs.

Since transtibial amputations differ by the region where the limb has been cut off, it is essential to develop an algorithm structure for different level amputees. Especially, the usability of the soleus muscle's EMG signal as neural network input is directly related to the distance between the knee and the amputation area. Because, if the amputation was applied to a place near to the knee, then recording an accurate EMG from the soleus muscle, which is widely used input in such system's algorithms,

may not be possible because of its location. Therefore, in this study two neural network structures are proposed for this specific need: TYPE II_{GRF-} and TYPE III_{GRF+}. In TYPE III_{GRF+} soleus muscle is not included as neural network input, on contrary to the TYPE II. Both of these structures generated position and moment estimation with high accuracy and low errors. Thus, outcomes of this study provide flexibility in the development of active ankle prosthesis such that the difference in amputation levels is not a limitation.

While building the shared database, ground reaction forces and EMG signals were recorded via sensor systems that cannot be embedded into a prosthetic device because of their size, price, and the intended use. Therefore, in the development of an active ankle prosthesis, different types of sensors will be needed. More importantly, to generate position and moment estimations, sensor outputs will be collected and evaluated using a microprocessor instead of data acquisition system and computer. Since, compared to microprocessors, these have advantages in terms of speed, resolution, quality recording, proposed neural network structures and algorithm should be tested with a component infrastructure that is more suitable for a prosthetic device to be embedded.

In summary, neural network based algorithms developed in this study showed that sensor infrastructure of an active ankle prosthesis can vary due to the amputation level of the user and design limitations. A device in which only EMG signals are used as network inputs requires 5 signals, collected from different muscles that are responsible for hip, knee and ankle movements. The EMG input number can be decreased to 3 if only EMG signals are recorded from tibialis anterior, soleus and gastrocnemius medialis muscles and a force or torque feedback is implemented into the system. These preliminary findings can initiate the development of an advanced active ankle prosthesis that mimics any ankle movements and can be comfortably used by amputees with all amputation levels.

4.2 Limitations And Future Studies

Although this thesis has reported a successful estimation of position and moment change in the ankle by using a neural network based algorithm; there is more work to be done to improve the current algorithm. Instead of using a literature based shared database, a new training database can be built to create an opportunity for developing an improved algorithm that estimates all kinds of ankle movements. According to the test results that obtained with the new database, outcomes of this study can be verified, or to overcome probable deficiencies an improvement on the current algorithm can be made. Consequently, a mechanical system that is suitable for the improved algorithm can be designed and produced.

APPENDIX A. NEURAL NETWORK RESULTS

In this chapter, neural network outputs for each test dataset are given.

A.1 TYPE I_{TP-} Outputs

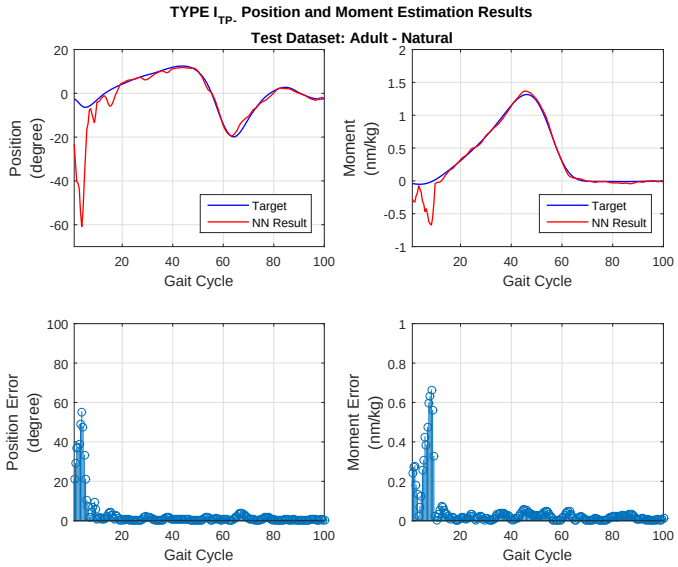

Figure A.1 TYPE I_{TP-} output when the 'Natural' speed class dataset of 'Adult' age group is given as input.

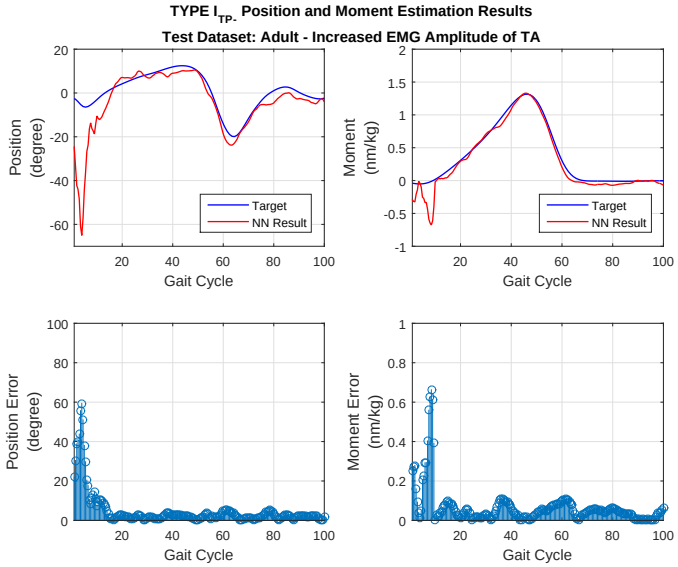

Figure A.2 TYPE I_{TP-} output when the 'Increased EMG Amplitude of TA' speed class dataset of 'Adult' age group is given as input.

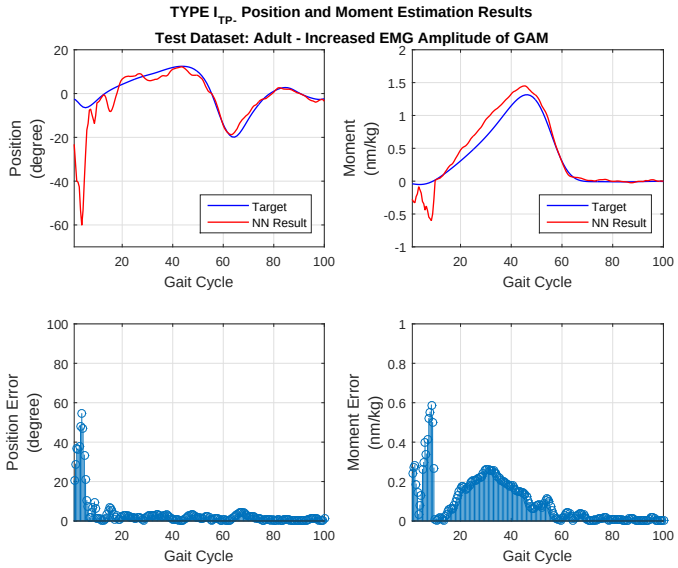

Figure A.3 TYPE I_{TP-} output when the 'Increased EMG Amplitude of GAM' speed class dataset of 'Adult' age group is given as input.

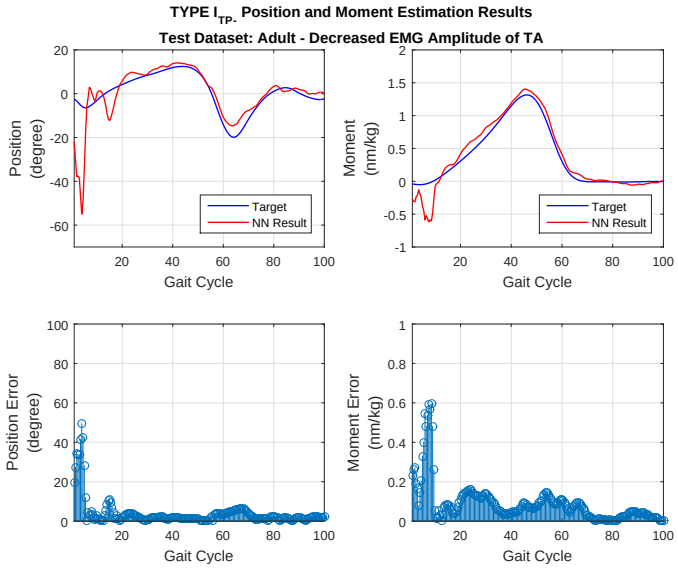

Figure A.4 TYPE I_{TP-} output when the 'Decreased EMG Amplitude of TA' speed class dataset of 'Adult' age group is given as input.

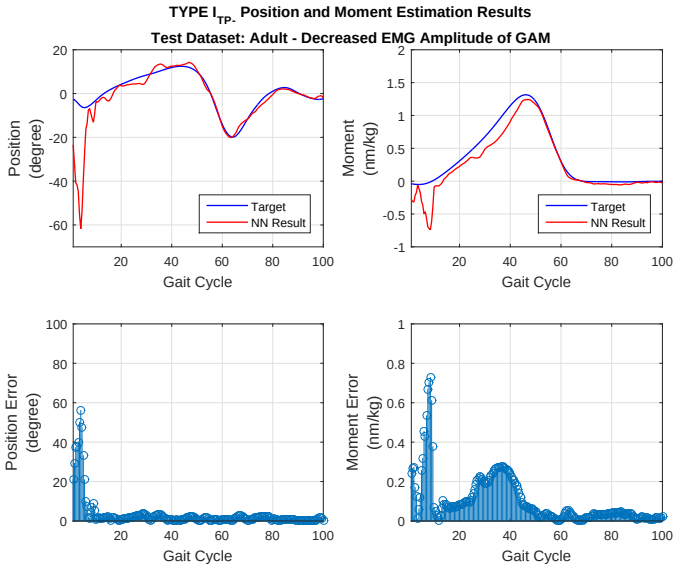

Figure A.5 TYPE I_{TP-} output when the 'Decreased EMG Amplitude of GAM' speed class dataset of 'Adult' age group is given as input.

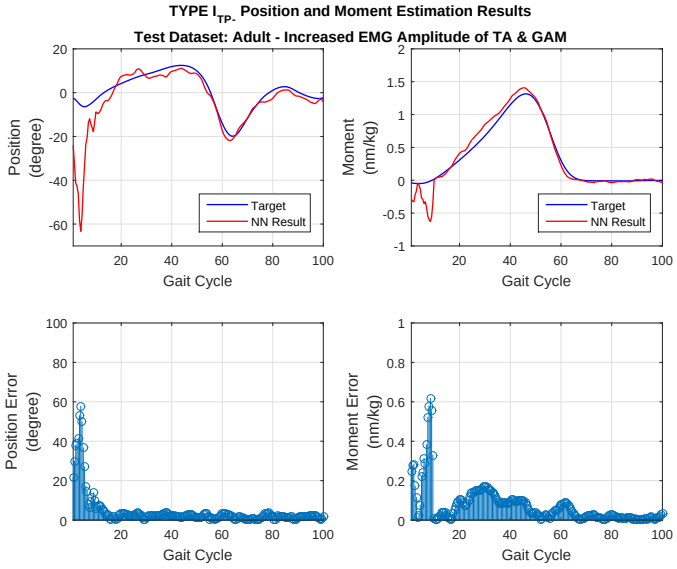

Figure A.6 TYPE I_{TP-} output when the 'Increased EMG Amplitude of TA and GAM' speed class dataset of 'Adult' age group is given as input.

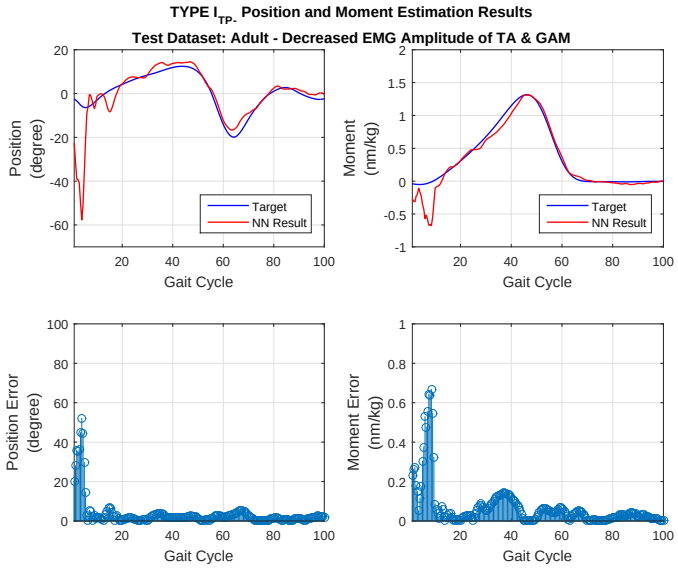

Figure A.7 TYPE I_{TP-} output when the 'Decreased EMG Amplitude of TA and GAM' speed class dataset of 'Adult' age group is given as input.

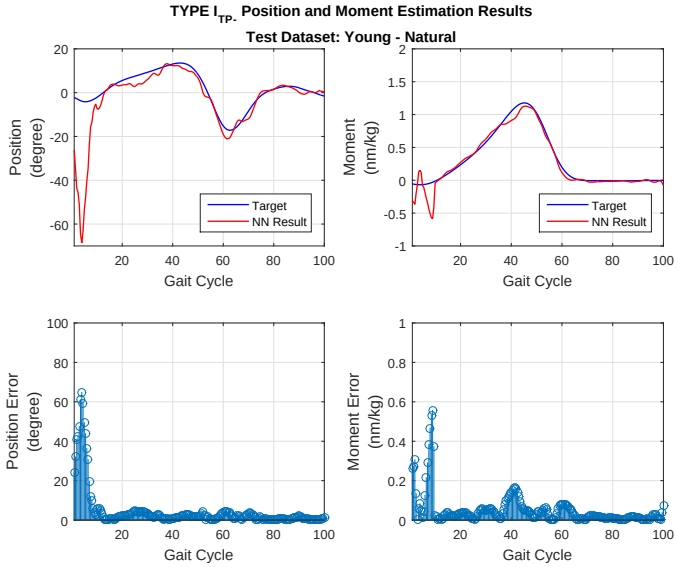

Figure A.8 TYPE I_{TP-} output when the 'Natural' speed class dataset of 'Young' age group is given as input.

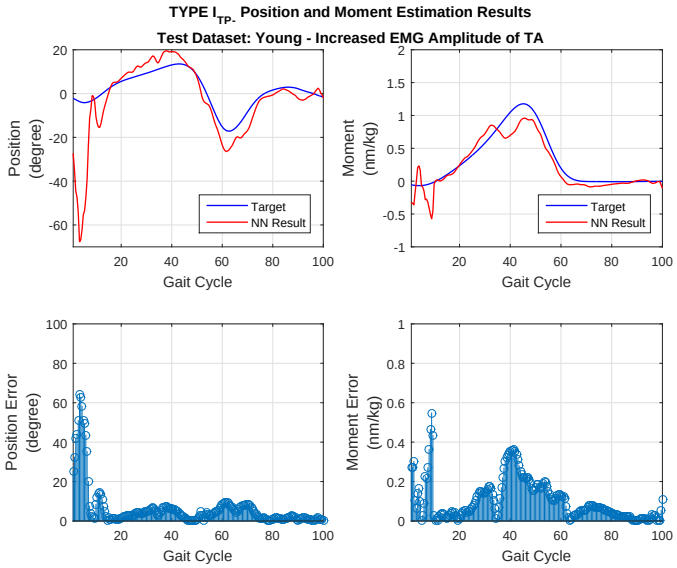

Figure A.9 TYPE I_{TP-} output when the 'Increased EMG Amplitude of TA' speed class dataset of 'Young' age group is given as input.

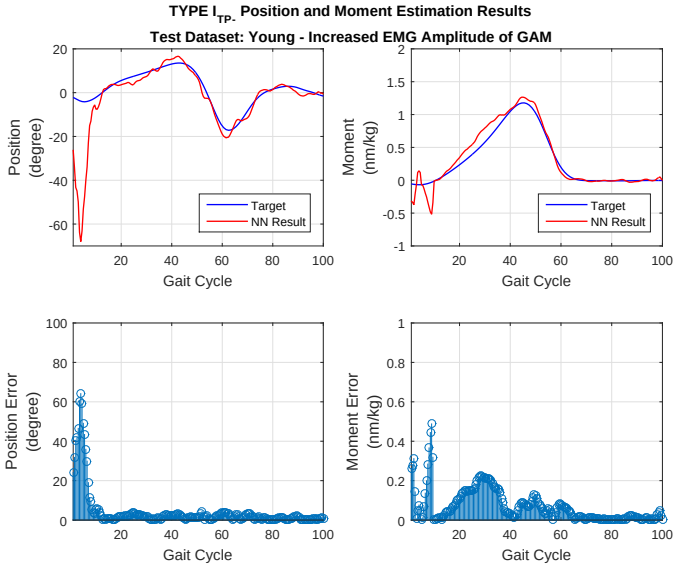

Figure A.10 TYPE I_{TP-} output when the 'Increased EMG Amplitude of GAM' speed class dataset of 'Young' age group is given as input.

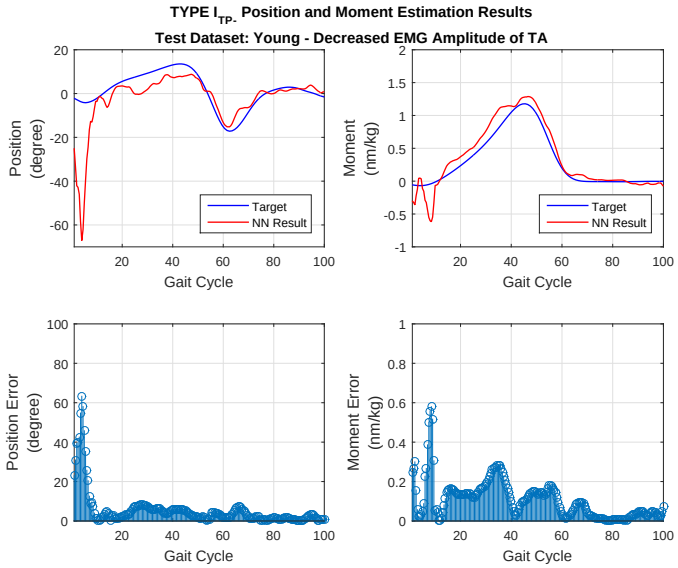

Figure A.11 TYPE I_{TP-} output when the 'Decreased EMG Amplitude of TA' speed class dataset of 'Young' age group is given as input.

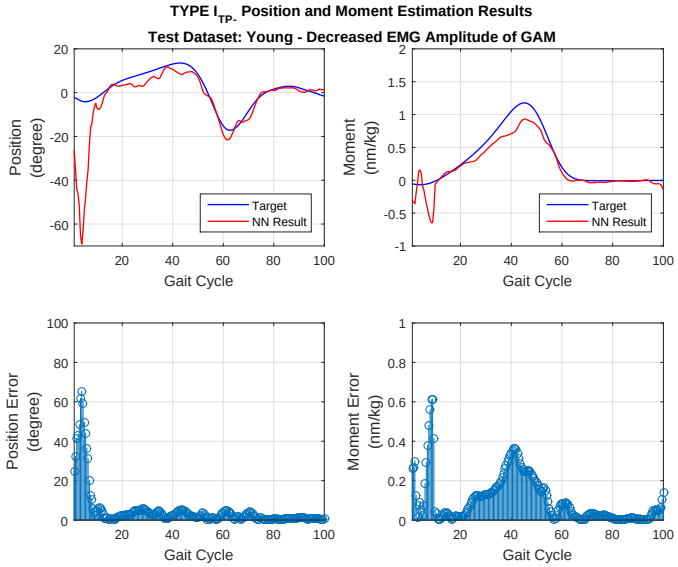

Figure A.12 TYPE I_{TP-} output when the 'Decreased EMG Amplitude of GAM' speed class dataset of 'Young' age group is given as input.

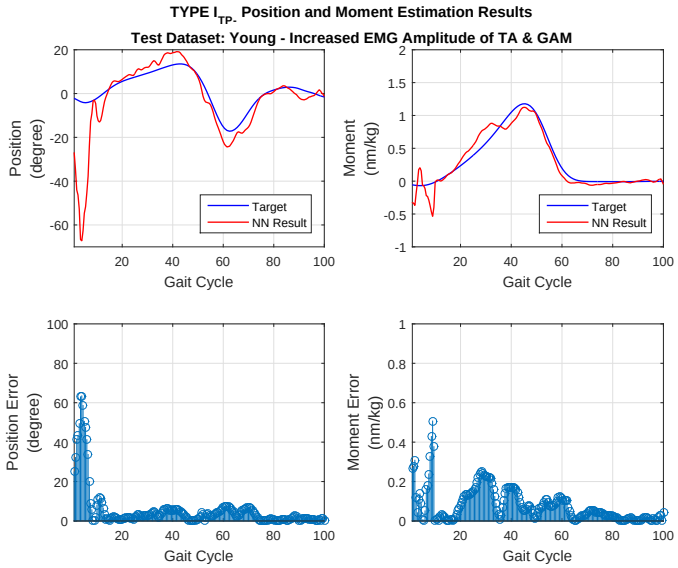

Figure A.13 TYPE I_{TP-} output when the 'Increased EMG Amplitude of TA and GAM' speed class dataset of 'Young' age group is given as input.

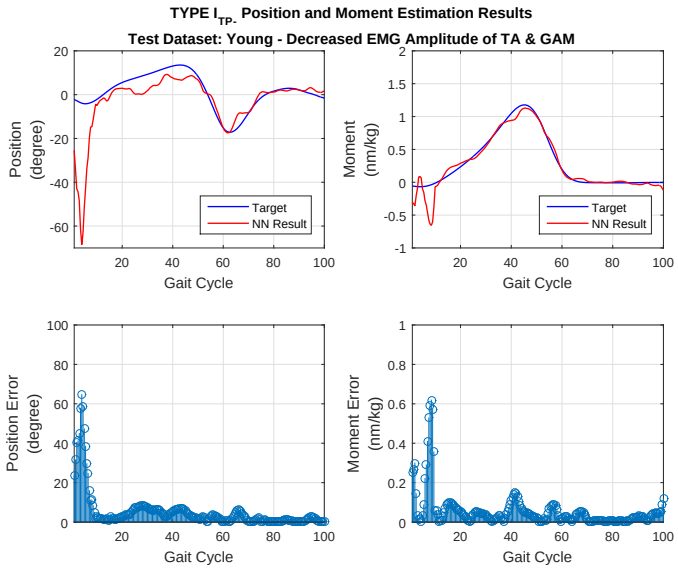

Figure A.14 TYPE I_{TP-} output when the 'Decreased EMG Amplitude of TA and GAM' speed class dataset of 'Young' age group is given as input.

A.2 TYPE I_{TP+} Outputs

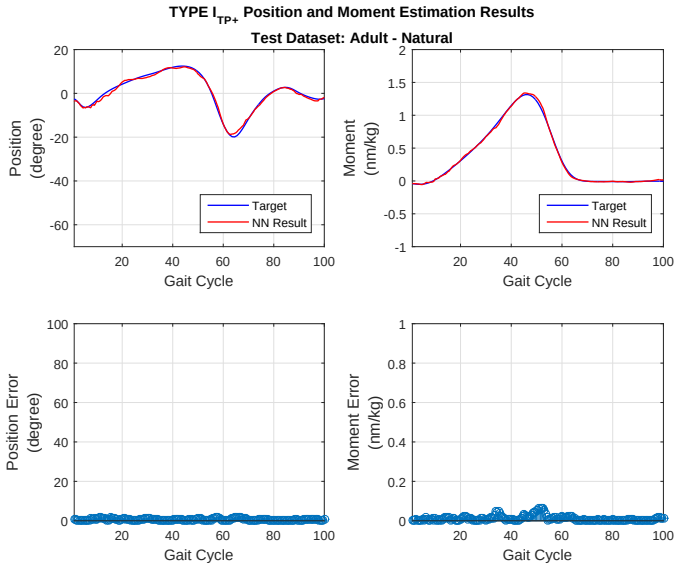

Figure A.15 TYPE I_{TP+} output when the 'Natural' speed class dataset of 'Adult' age group is given as input.

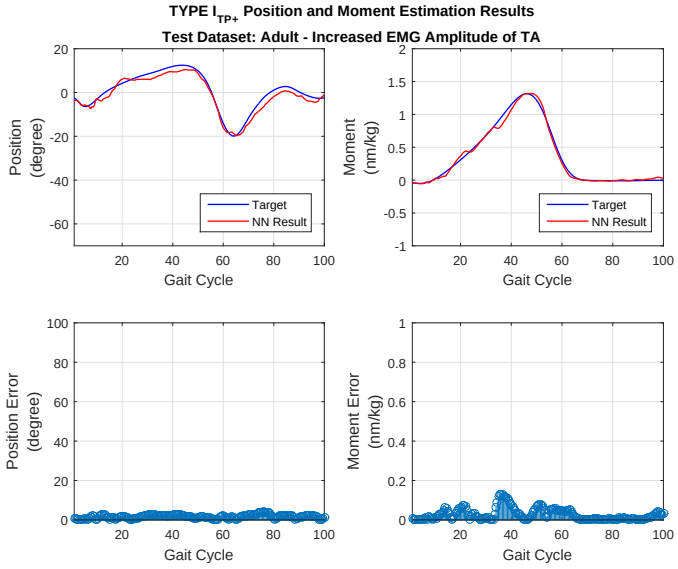

Figure A.16 TYPE I_{TP+} output when the 'Increased EMG Amplitude of TA' speed class dataset of 'Adult' age group is given as input.

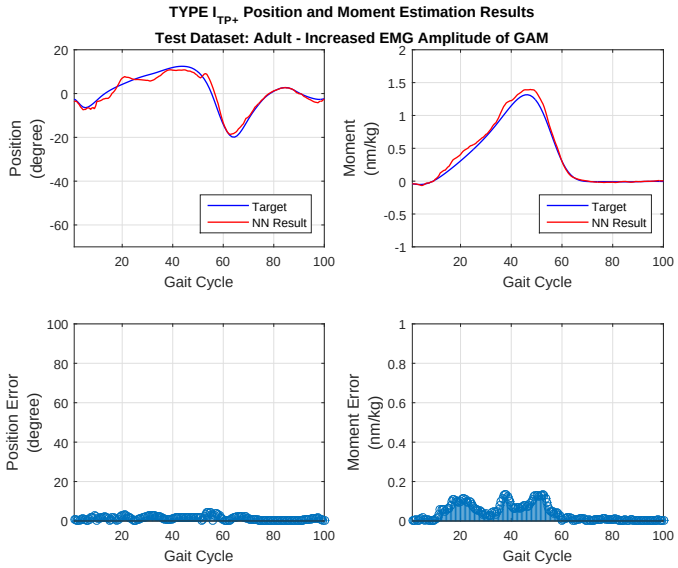

Figure A.17 TYPE I_{TP+} output when the 'Increased EMG Amplitude of GAM' speed class dataset of 'Adult' age group is given as input.

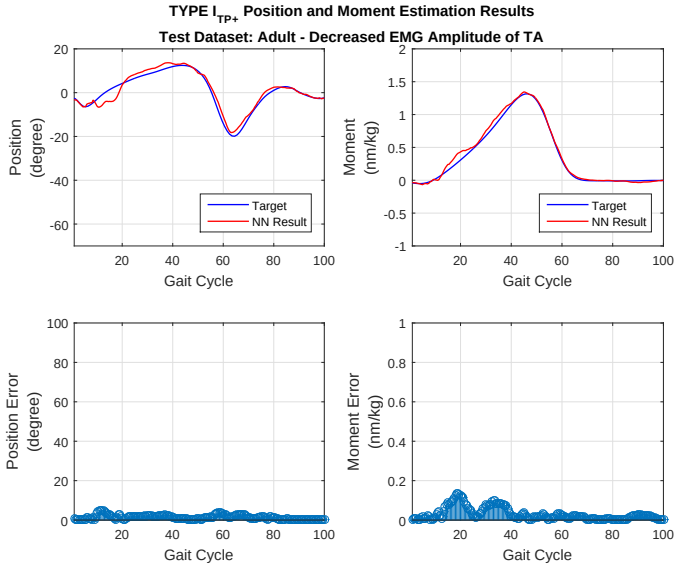

Figure A.18 TYPE I_{TP+} output when the 'Decreased EMG Amplitude of TA' speed class dataset of 'Adult' age group is given as input.

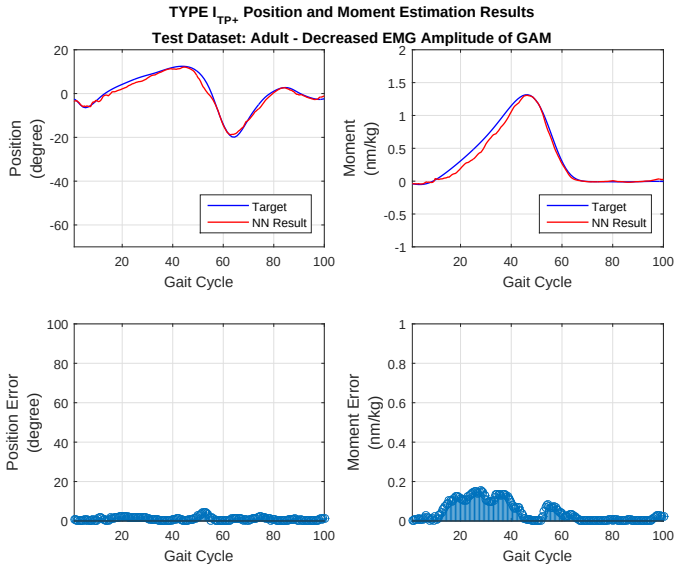

Figure A.19 TYPE I_{TP+} output when the 'Decreased EMG Amplitude of GAM' speed class dataset of 'Adult' age group is given as input.

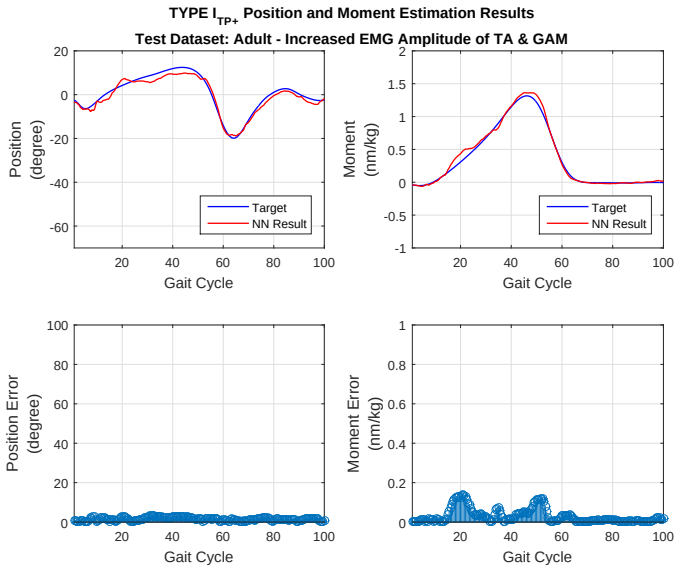

Figure A.20 TYPE I_{TP+} output when the 'Increased EMG Amplitude of TA and GAM' speed class dataset of 'Adult' age group is given as input.

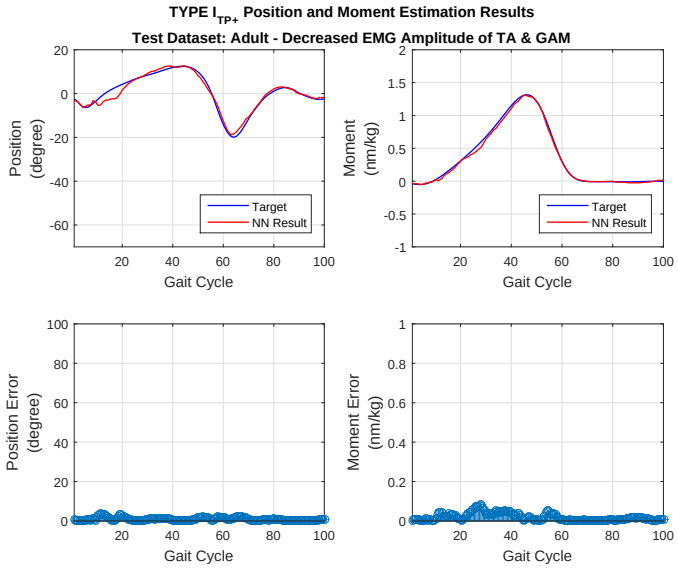

Figure A.21 TYPE I_{TP+} output when the 'Decreased EMG Amplitude of TA and GAM' speed class dataset of 'Adult' age group is given as input.

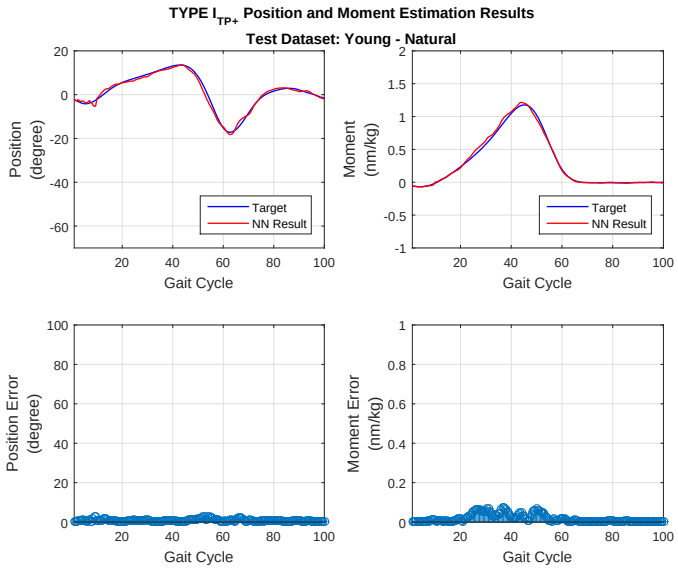

Figure A.22 TYPE I_{TP+} output when the 'Natural' speed class dataset of 'Young' age group is given as input.

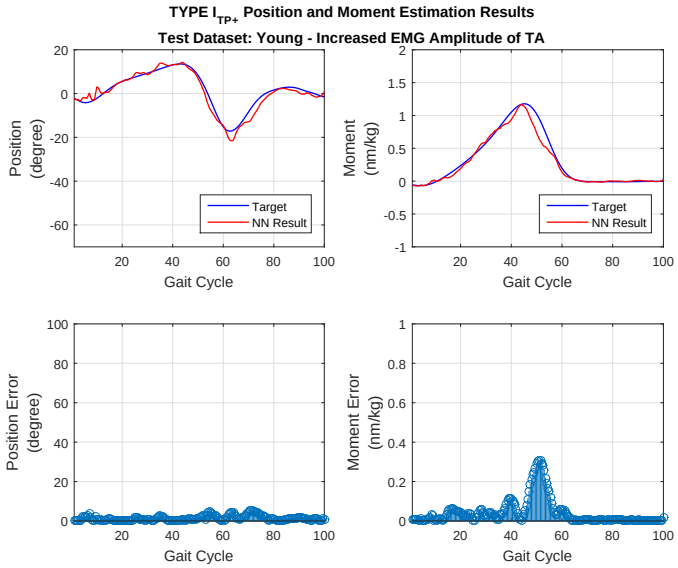

Figure A.23 TYPE I_{TP+} output when the 'Increased EMG Amplitude of TA' speed class dataset of 'Young' age group is given as input.

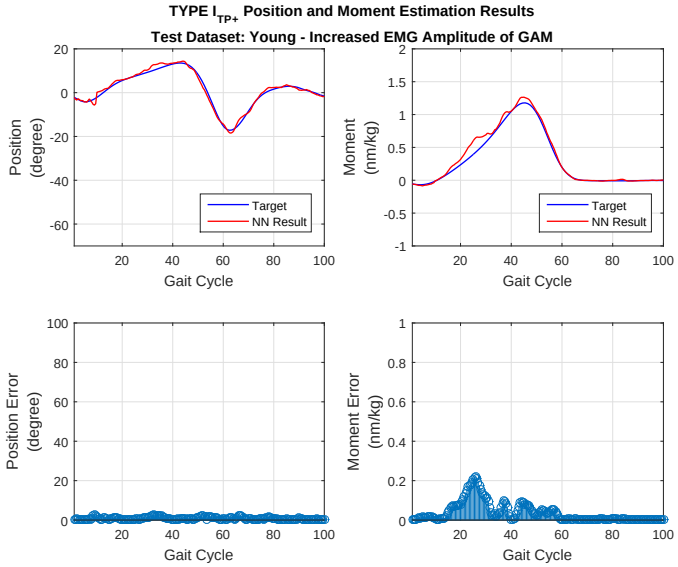

Figure A.24 TYPE I_{TP+} output when the 'Increased EMG Amplitude of GAM' speed class dataset of 'Young' age group is given as input.

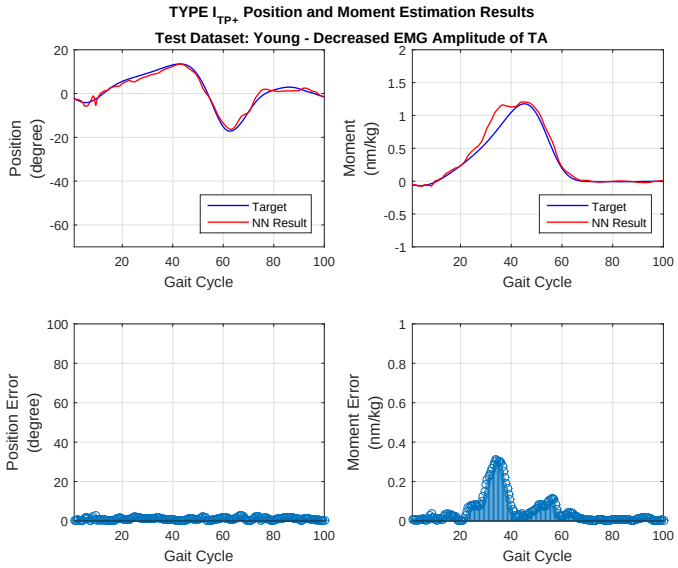

Figure A.25 TYPE I_{TP+} output when the 'Decreased EMG Amplitude of TA' speed class dataset of 'Young' age group is given as input.

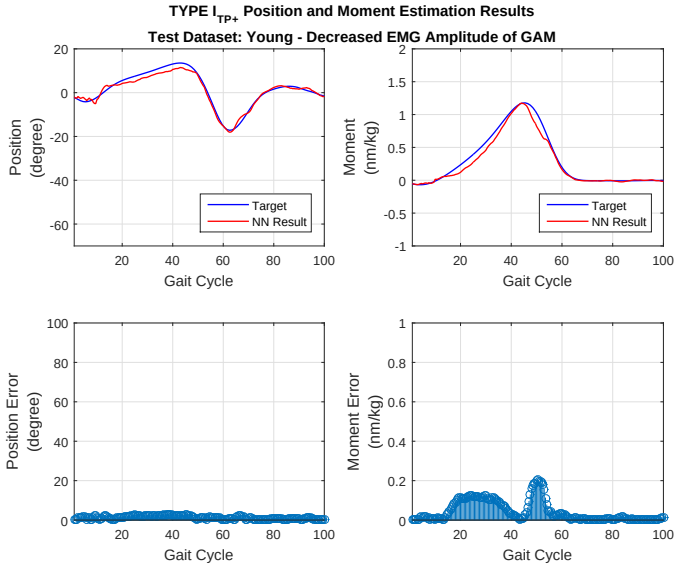

Figure A.26 TYPE I_{TP+} output when the 'Decreased EMG Amplitude of GAM' speed class dataset of 'Young' age group is given as input.

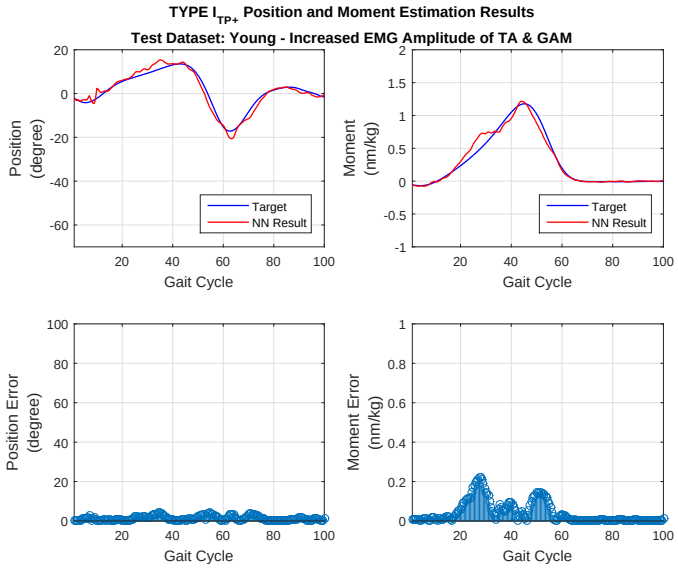

Figure A.27 TYPE I_{TP+} output when the 'Increased EMG Amplitude of TA and GAM' speed class dataset of 'Young' age group is given as input.

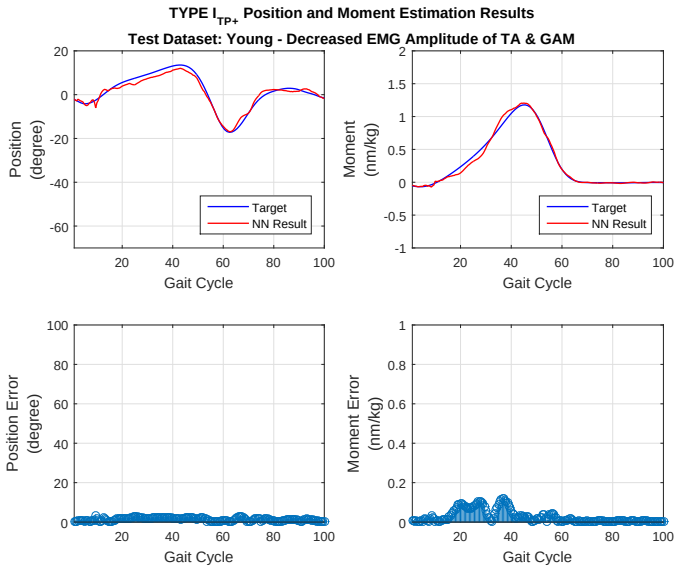

Figure A.28 TYPE I_{TP+} output when the 'Decreased EMG Amplitude of TA and GAM' speed class dataset of 'Young' age group is given as input.

A.3 TYPE II$_{GRF-}$ Outputs

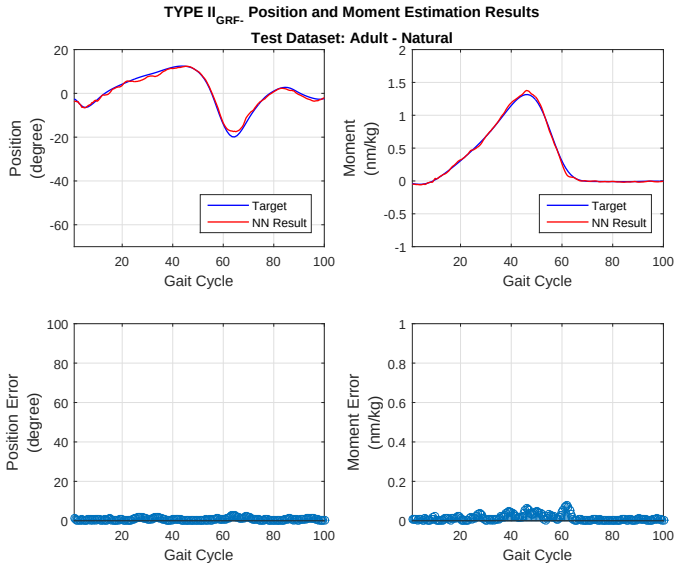

Figure A.29 TYPE II$_{GRF-}$ output when the 'Natural' speed class dataset of 'Adult' age group is given as input.

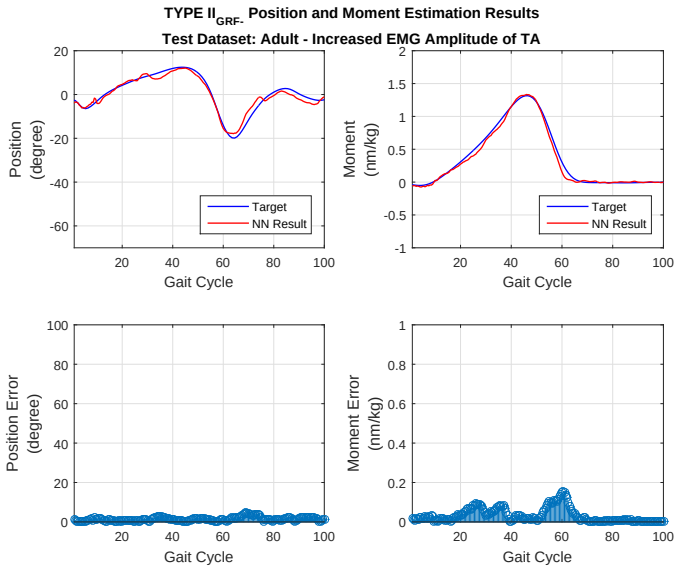

Figure A.30 TYPE II$_{GRF-}$ output when the 'Increased EMG Amplitude of TA' speed class dataset of 'Adult' age group is given as input.

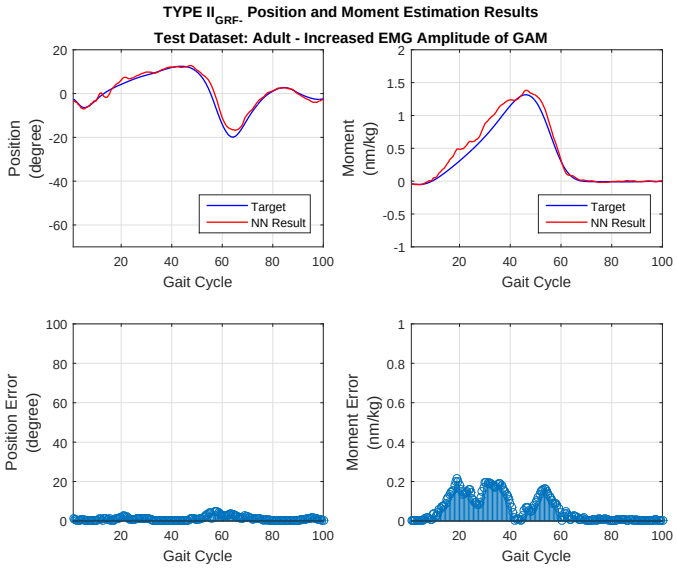

Figure A.31 TYPE II_{GRF-} output when the 'Increased EMG Amplitude of GAM' speed class dataset of 'Adult' age group is given as input.

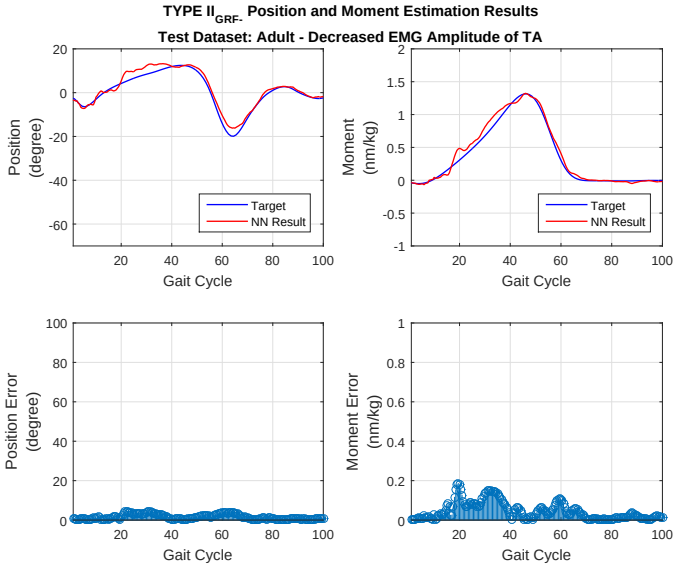

Figure A.32 TYPE II_{GRF-} output when the 'Decreased EMG Amplitude of TA' speed class dataset of 'Adult' age group is given as input.

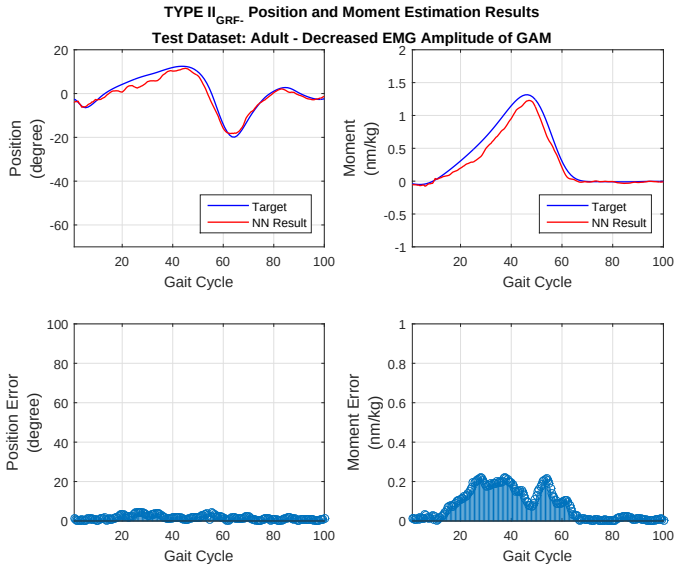

Figure A.33 TYPE II_{GRF-} output when the 'Decreased EMG Amplitude of GAM' speed class dataset of 'Adult' age group is given as input.

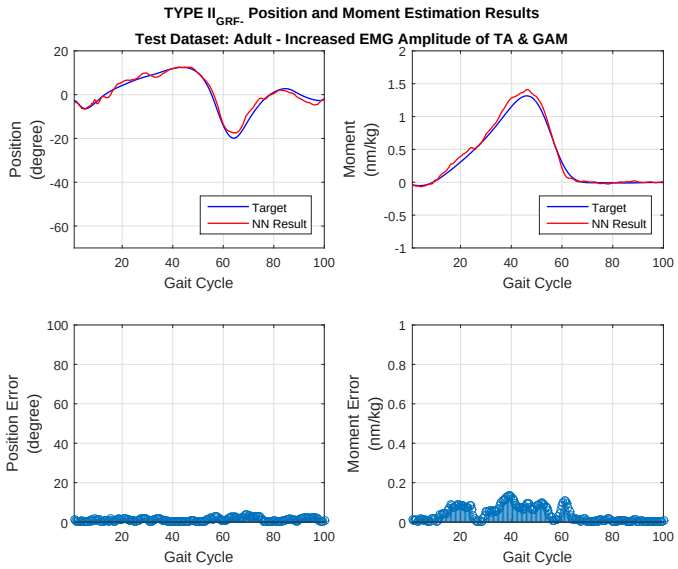

Figure A.34 TYPE II_{GRF-} output when the 'Increased EMG Amplitude of TA and GAM' speed class dataset of 'Adult' age group is given as input.

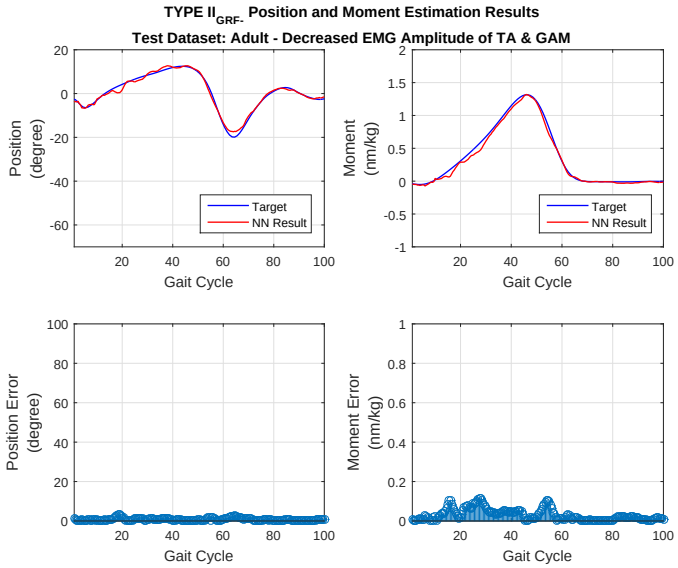

Figure A.35 TYPE II_{GRF-} output when the 'Decreased EMG Amplitude of TA and GAM' speed class dataset of 'Adult' age group is given as input.

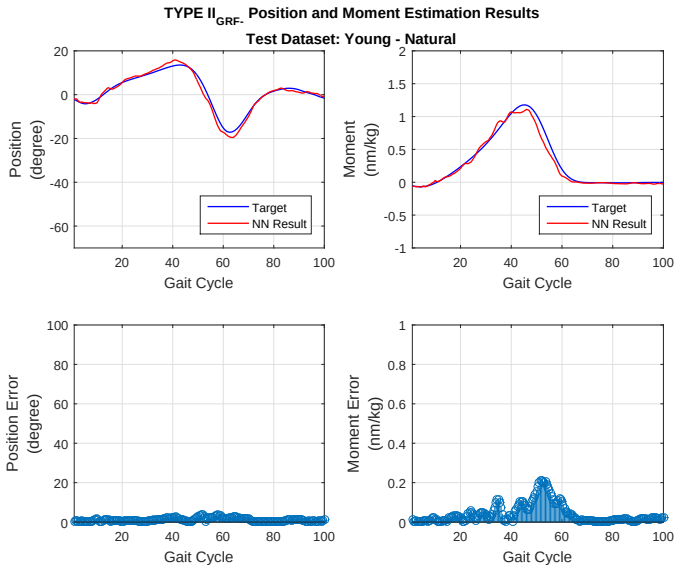

Figure A.36 TYPE II_{GRF-} output when the 'Natural' speed class dataset of 'Young' age group is given as input.

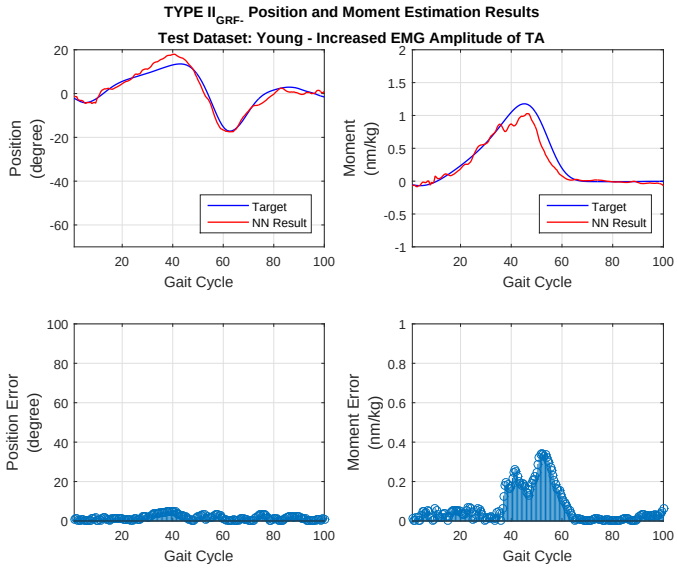

Figure A.37 TYPE II_{GRF-} output when the 'Increased EMG Amplitude of TA' speed class dataset of 'Young' age group is given as input.

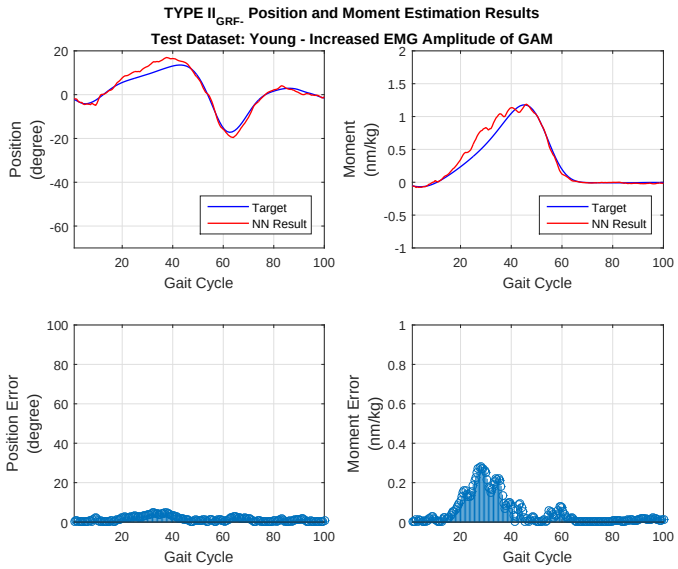

Figure A.38 TYPE II_{GRF-} output when the 'Increased EMG Amplitude of GAM' speed class dataset of 'Young' age group is given as input.

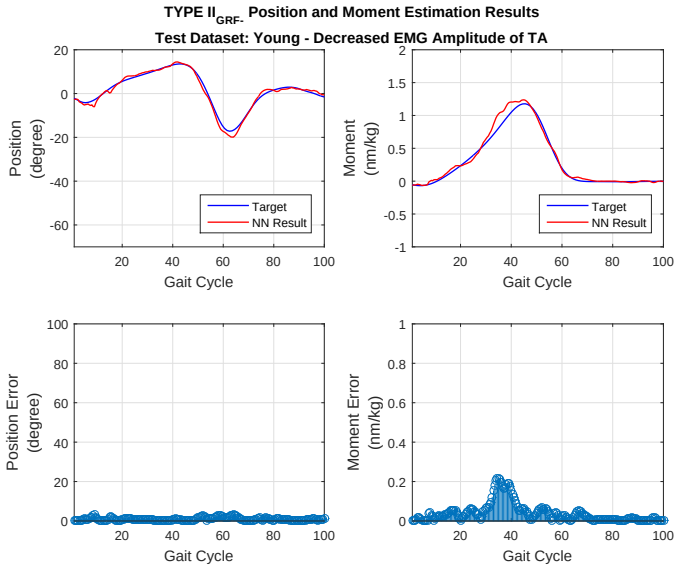

Figure A.39 TYPE II_{GRF-} output when the 'Decreased EMG Amplitude of TA' speed class dataset of 'Young' age group is given as input.

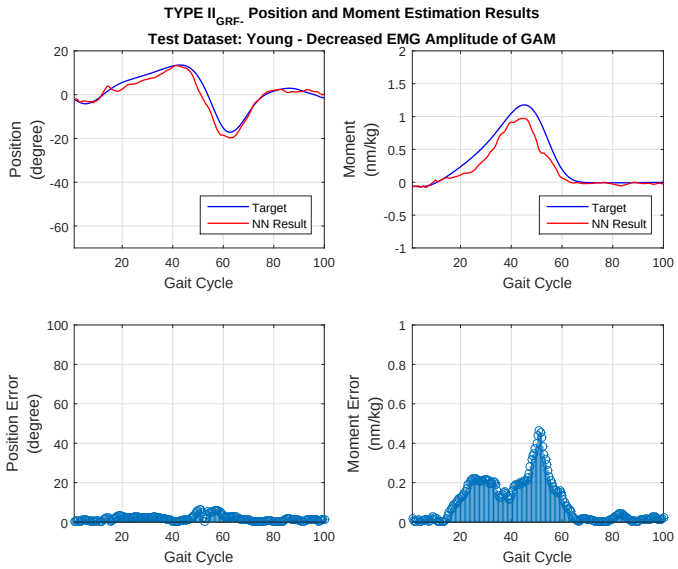

Figure A.40 TYPE II_{GRF-} output when the 'Decreased EMG Amplitude of GAM' speed class dataset of 'Young' age group is given as input.

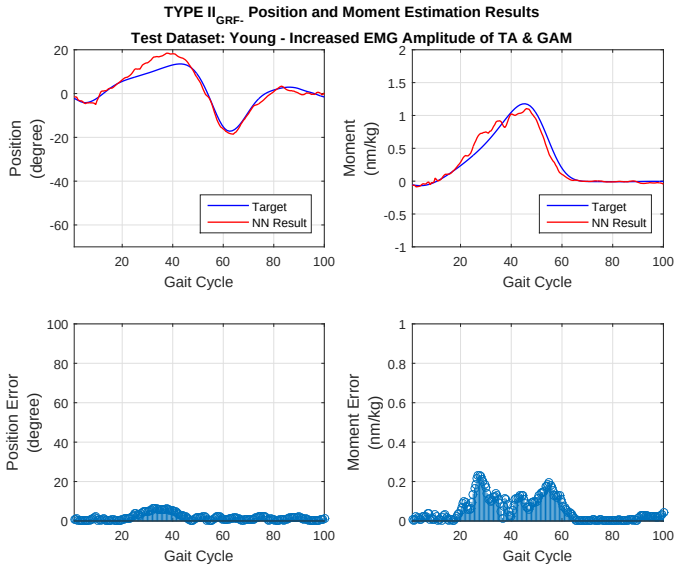

Figure A.41 TYPE II_{GRF-} output when the 'Increased EMG Amplitude of TA and GAM' speed class dataset of 'Young' age group is given as input.

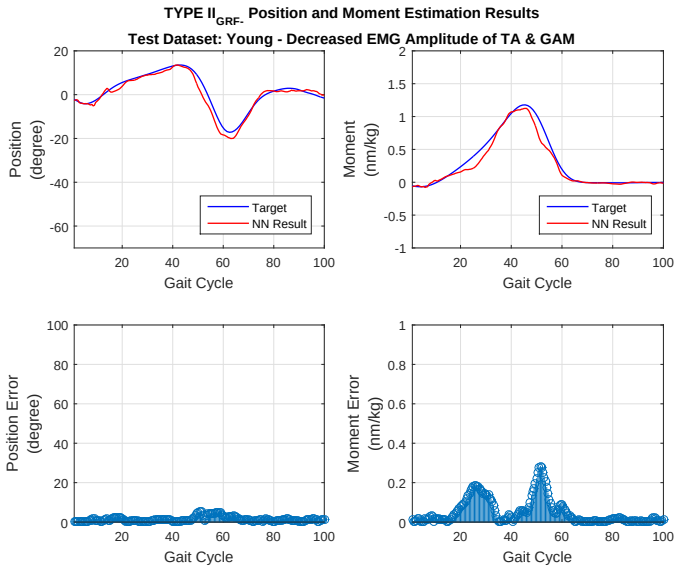

Figure A.42 TYPE II_{GRF-} output when the 'Decreased EMG Amplitude of TA and GAM' speed class dataset of 'Young' age group is given as input.

A.4 TYPE III$_{GRF-}$ Outputs

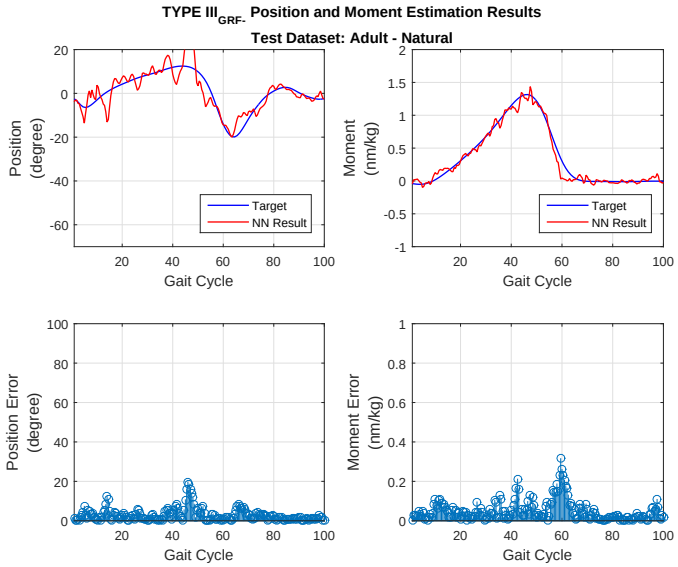

Figure A.43 TYPE III$_{GRF-}$ output when the 'Natural' speed class dataset of 'Adult' age group is given as input.

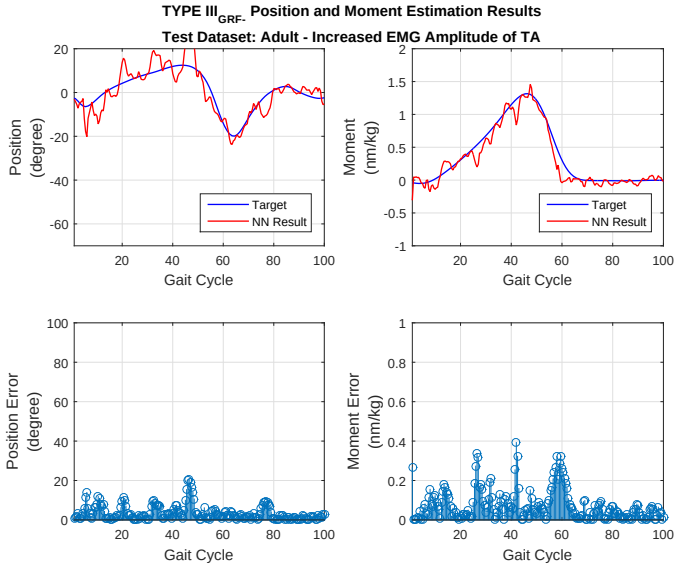

Figure A.44 TYPE III$_{GRF-}$ output when the 'Increased EMG Amplitude of TA' speed class dataset of 'Adult' age group is given as input.

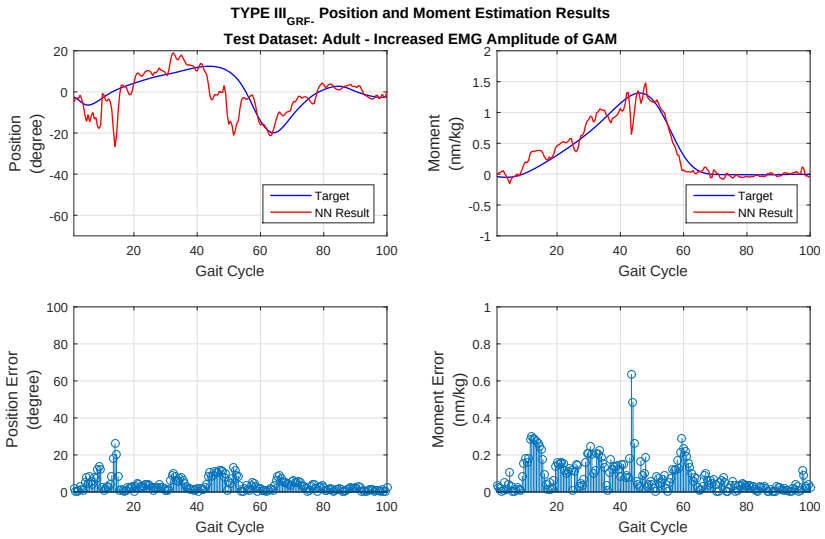

Figure A.45 TYPE III_{GRF-} output when the 'Increased EMG Amplitude of GAM' speed class dataset of 'Adult' age group is given as input.

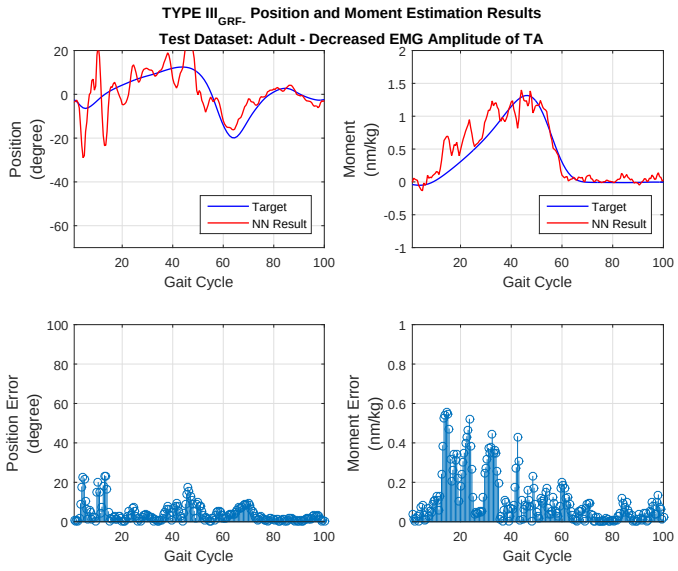

Figure A.46 TYPE III_{GRF-} output when the 'Decreased EMG Amplitude of TA' speed class dataset of 'Adult' age group is given as input.

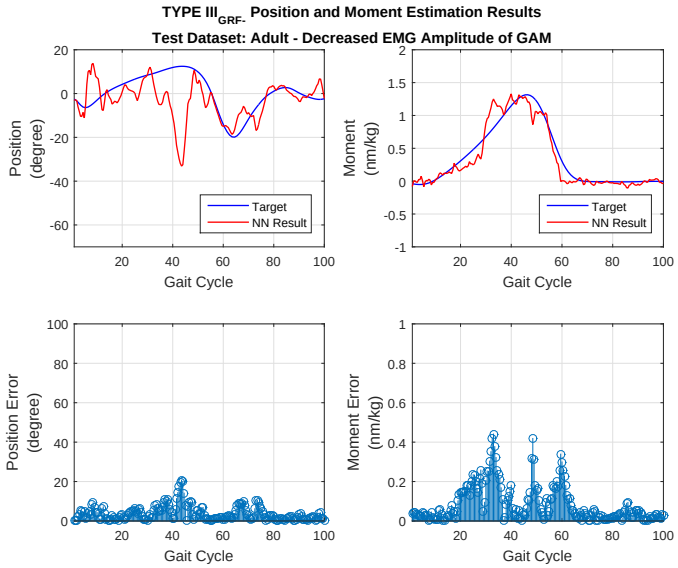

Figure A.47 TYPE III_{GRF-} output when the 'Decreased EMG Amplitude of GAM' speed class dataset of 'Adult' age group is given as input.

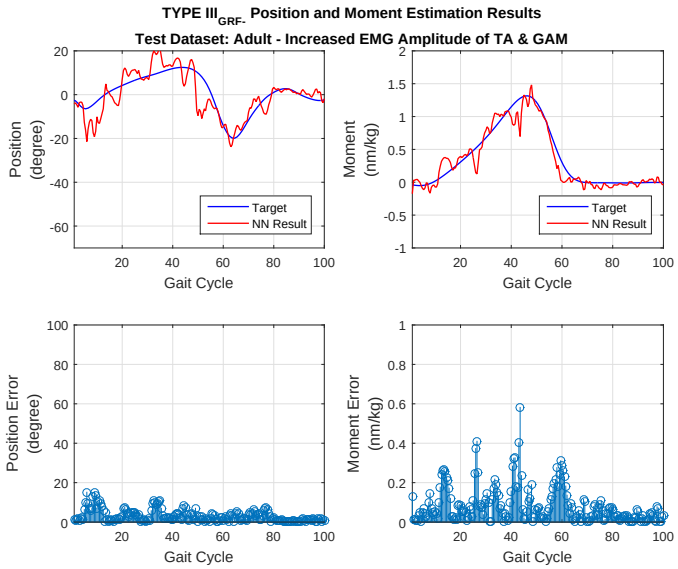

Figure A.48 TYPE III_{GRF-} output when the 'Increased EMG Amplitude of TA and GAM' speed class dataset of 'Adult' age group is given as input.

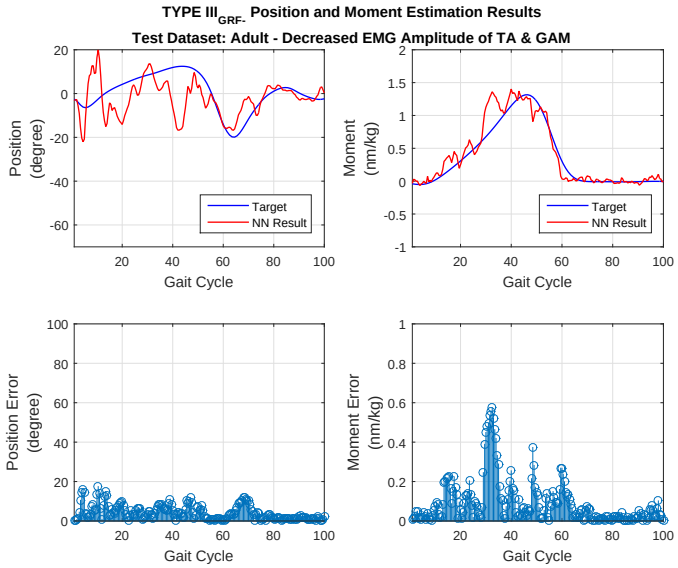

Figure A.49 TYPE III_{GRF-} output when the 'Decreased EMG Amplitude of TA and GAM' speed class dataset of 'Adult' age group is given as input.

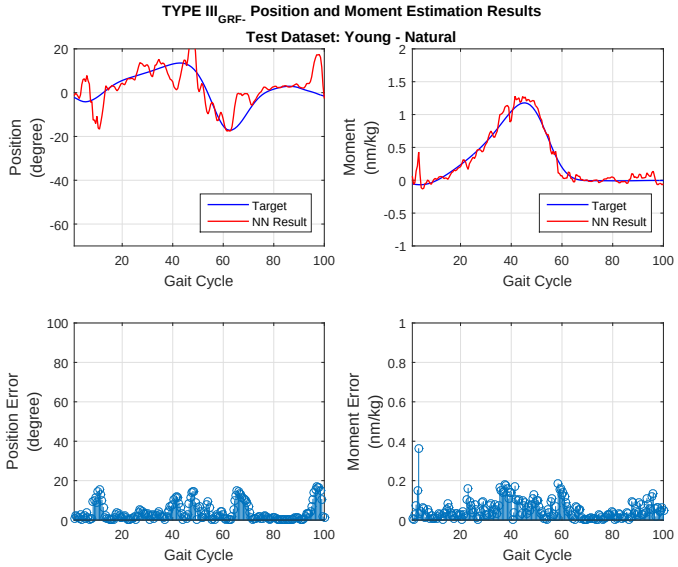

Figure A.50 TYPE III_{GRF-} output when the 'Natural' speed class dataset of 'Young' age group is given as input.

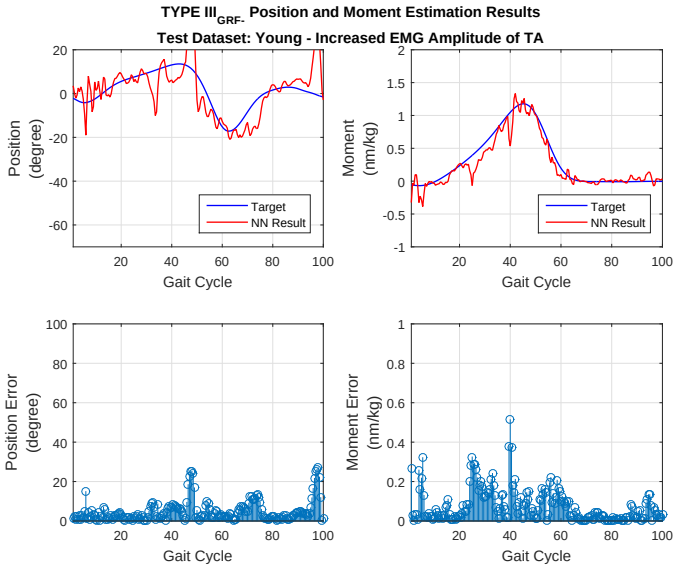

Figure A.51 TYPE III_{GRF-} output when the 'Increased EMG Amplitude of TA' speed class dataset of 'Young' age group is given as input.

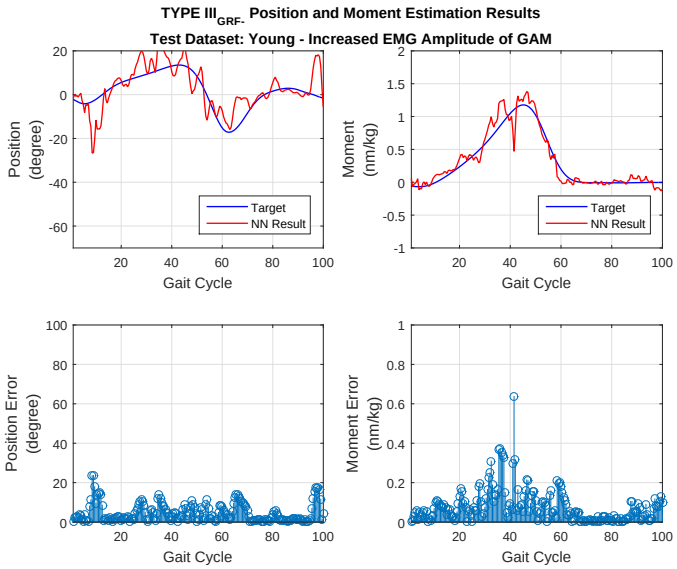

Figure A.52 TYPE III_{GRF-} output when the 'Increased EMG Amplitude of GAM' speed class dataset of 'Young' age group is given as input.

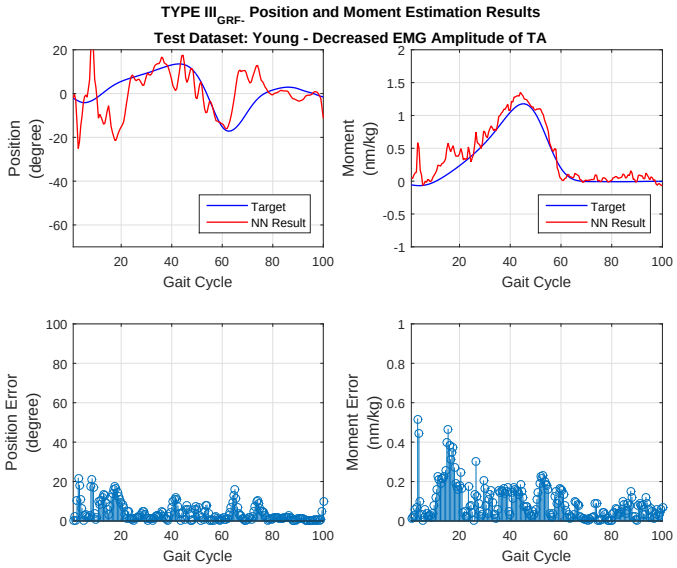

Figure A.53 TYPE III_{GRF-} output when the 'Decreased EMG Amplitude of TA' speed class dataset of 'Young' age group is given as input.

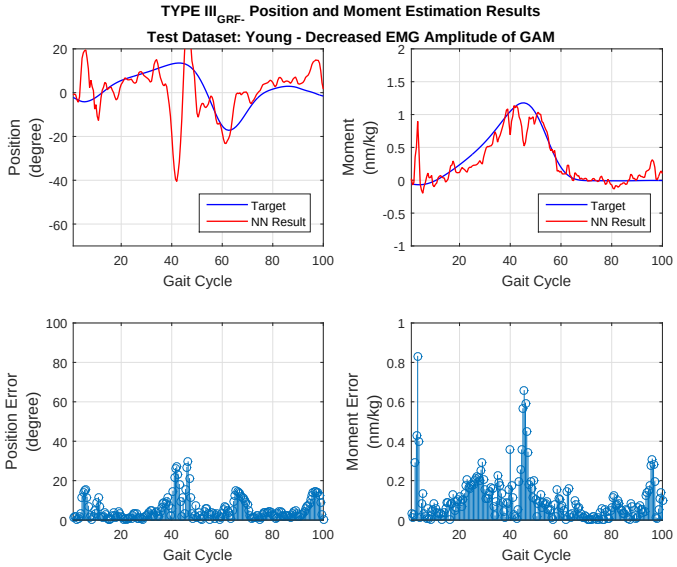

Figure A.54 TYPE III_{GRF-} output when the 'Decreased EMG Amplitude of GAM' speed class dataset of 'Young' age group is given as input.

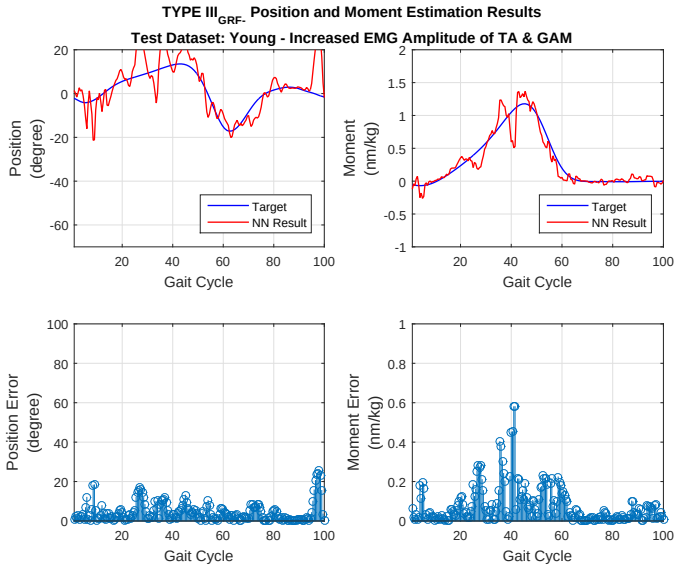

Figure A.55 TYPE III_{GRF-} output when the 'Increased EMG Amplitude of TA and GAM' speed class dataset of 'Young' age group is given as input.

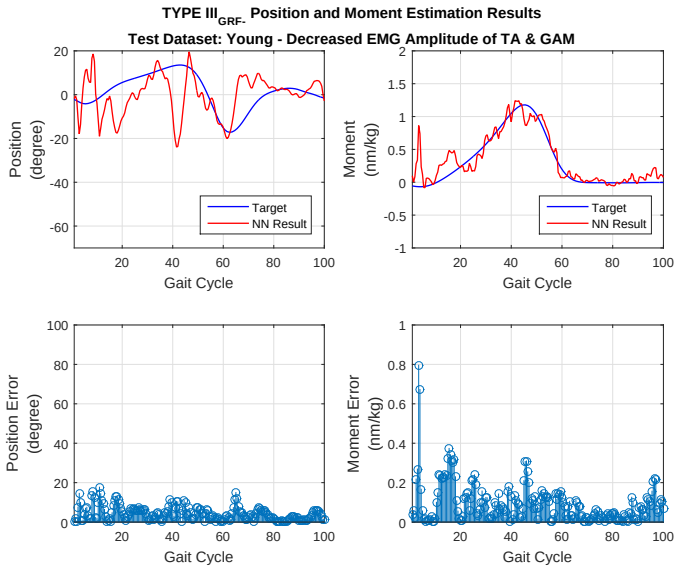

Figure A.56 TYPE III_{GRF-} output when the 'Decreased EMG Amplitude of TA and GAM' speed class dataset of 'Young' age group is given as input.

A.5 TYPE III$_{GRF+}$ Outputs

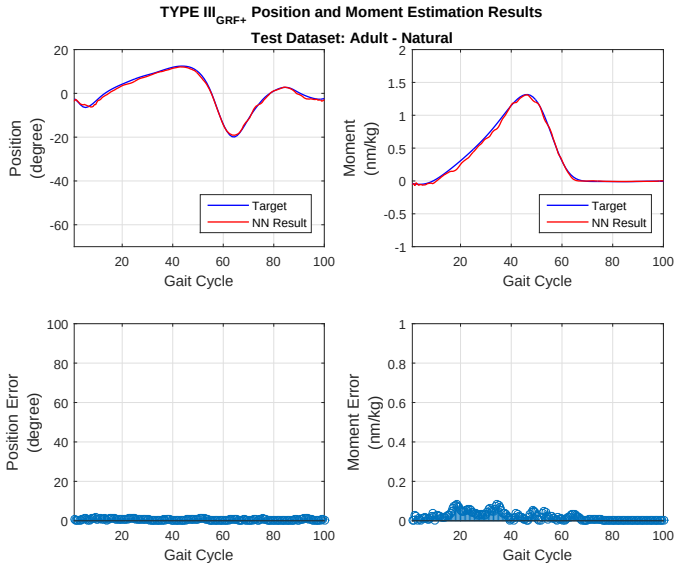

Figure A.57 TYPE III$_{GRF+}$ output when the 'Natural' speed class dataset of 'Adult' age group is given as input.

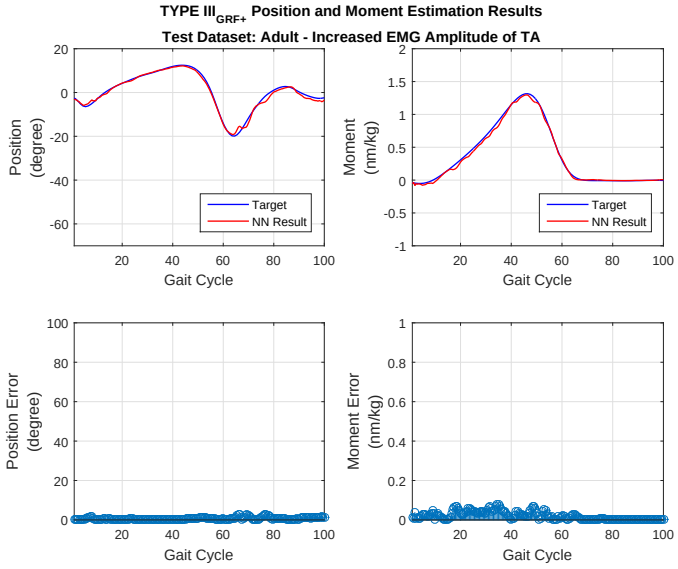

Figure A.58 TYPE III$_{GRF+}$ output when the 'Increased EMG Amplitude of TA' speed class dataset of 'Adult' age group is given as input.

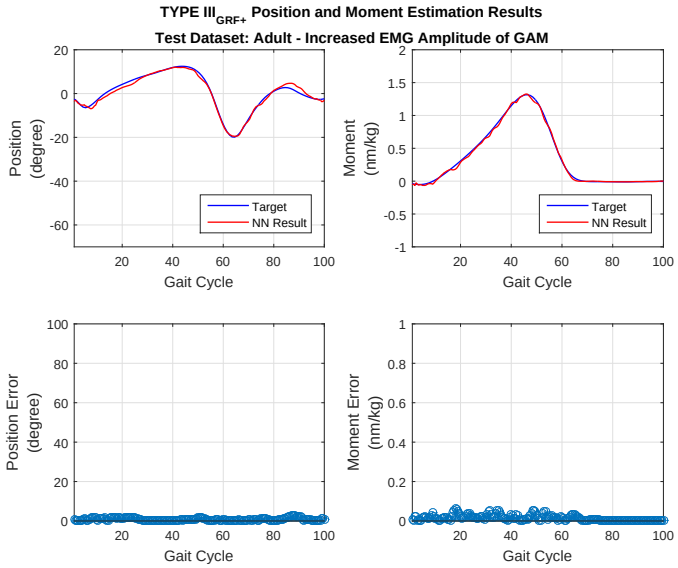

Figure A.59 TYPE III_{GRF+} output when the 'Increased EMG Amplitude of GAM' speed class dataset of 'Adult' age group is given as input.

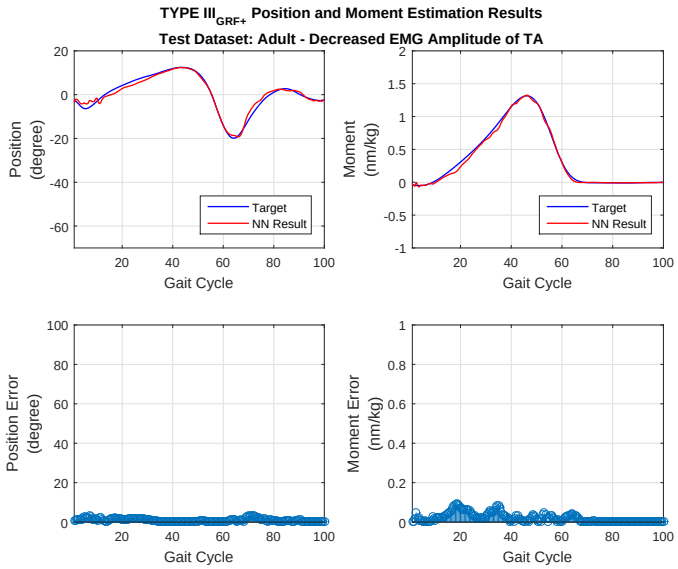

Figure A.60 TYPE III_{GRF+} output when the 'Decreased EMG Amplitude of TA' speed class dataset of 'Adult' age group is given as input.

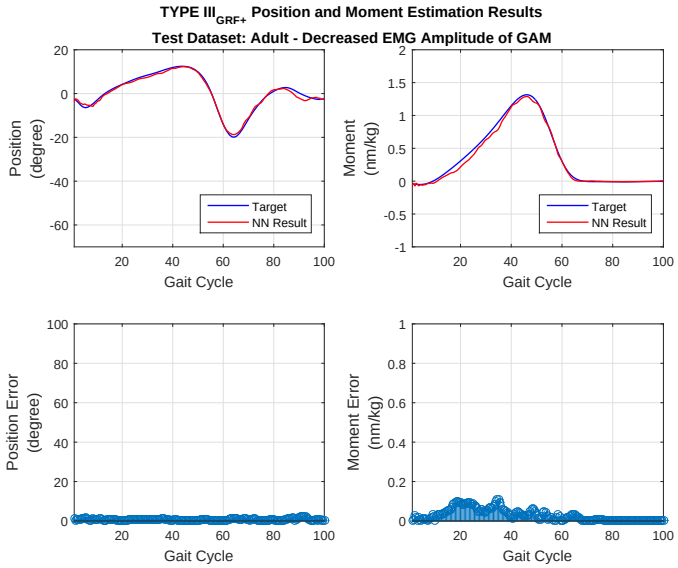

Figure A.61 TYPE III$_{GRF+}$ output when the 'Decreased EMG Amplitude of GAM' speed class dataset of 'Adult' age group is given as input.

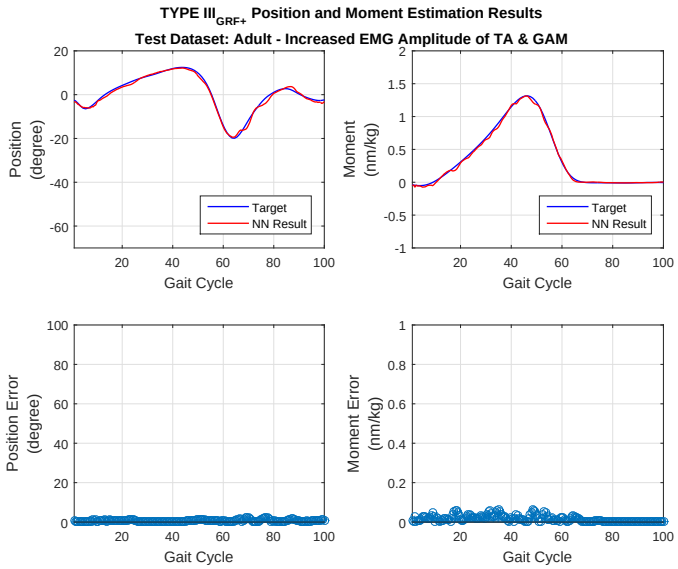

Figure A.62 TYPE III$_{GRF+}$ output when the 'Increased EMG Amplitude of TA and GAM' speed class dataset of 'Adult' age group is given as input.

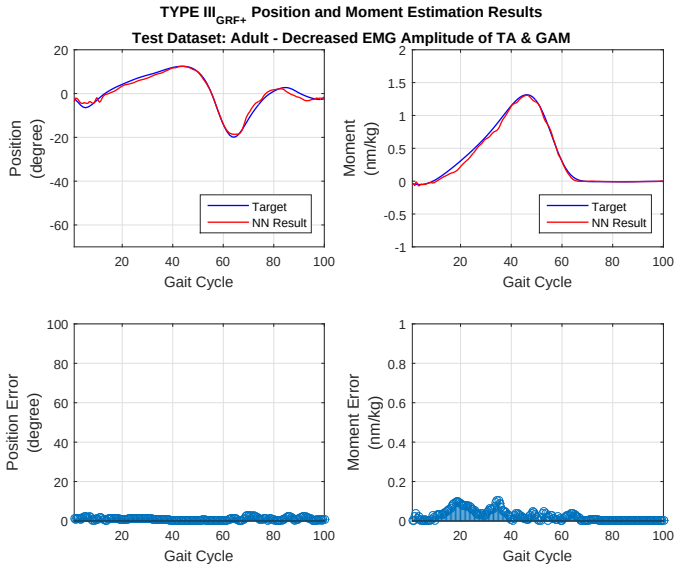

Figure A.63 TYPE III$_{GRF+}$ output when the 'Decreased EMG Amplitude of TA and GAM' speed class dataset of 'Adult' age group is given as input.

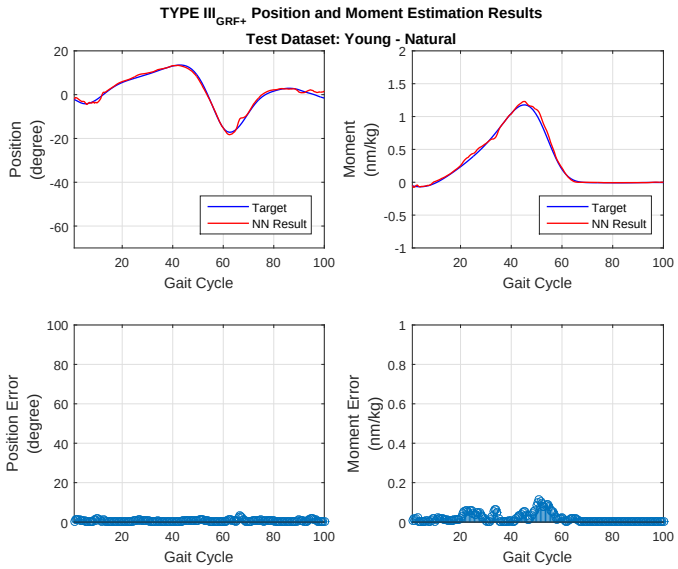

Figure A.64 TYPE III$_{GRF+}$ output when the 'Natural' speed class dataset of 'Young' age group is given as input.

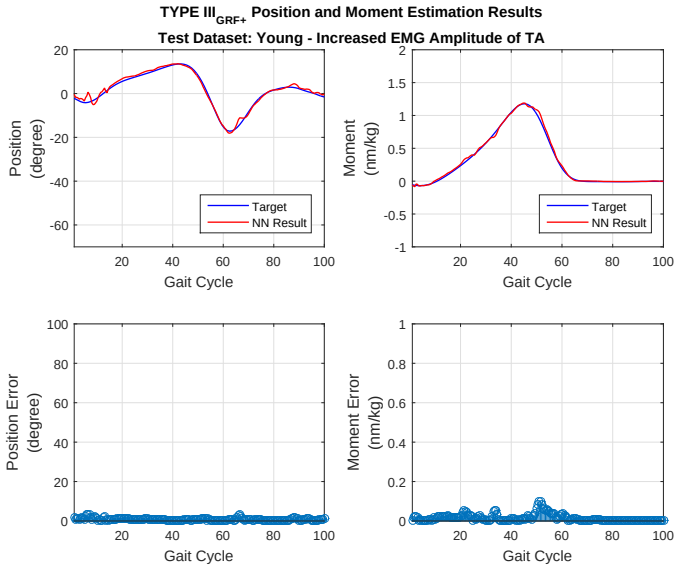

Figure A.65 TYPE III_{GRF+} output when the 'Increased EMG Amplitude of TA' speed class dataset of 'Young' age group is given as input.

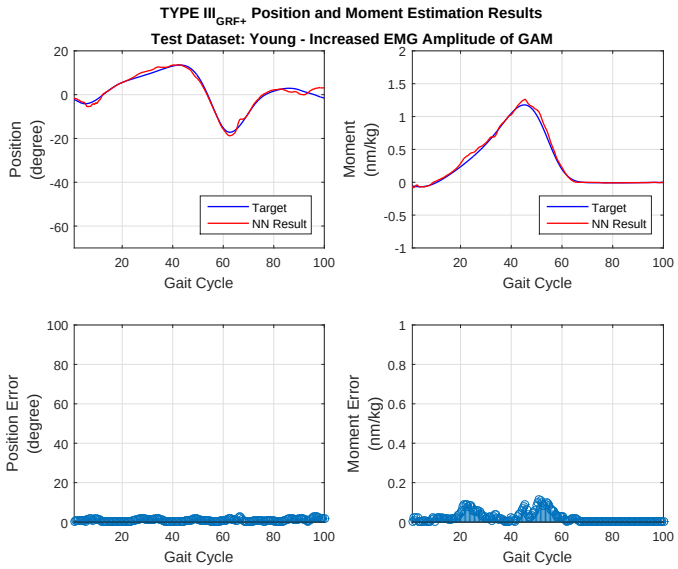

Figure A.66 TYPE III_{GRF+} output when the 'Increased EMG Amplitude of GAM' speed class dataset of 'Young' age group is given as input.

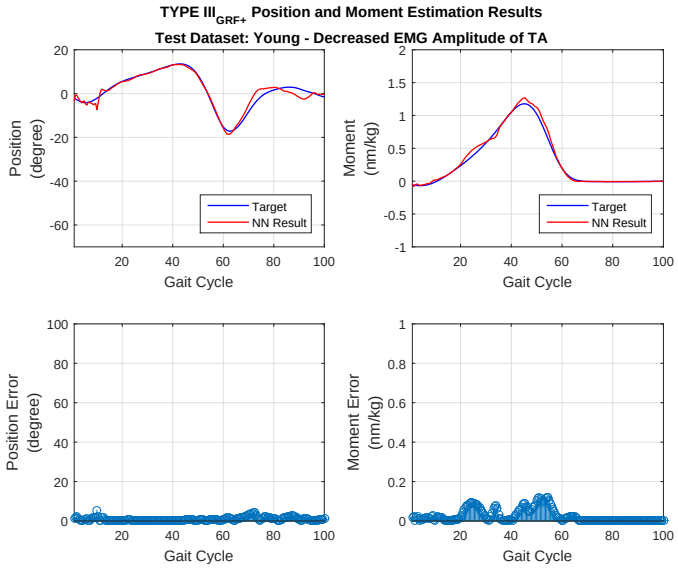

Figure A.67 TYPE $\text{III}_{\text{GRF+}}$ output when the 'Decreased EMG Amplitude of TA' speed class dataset of 'Young' age group is given as input.

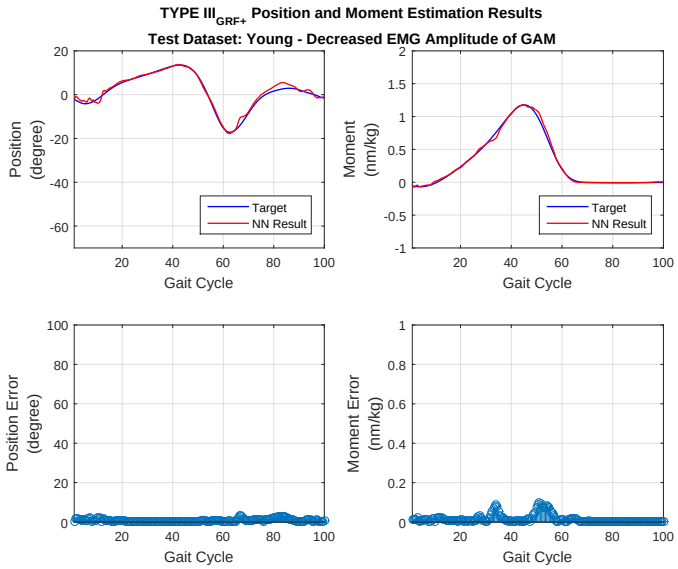

Figure A.68 TYPE $\text{III}_{\text{GRF+}}$ output when the 'Decreased EMG Amplitude of GAM' speed class dataset of 'Young' age group is given as input.

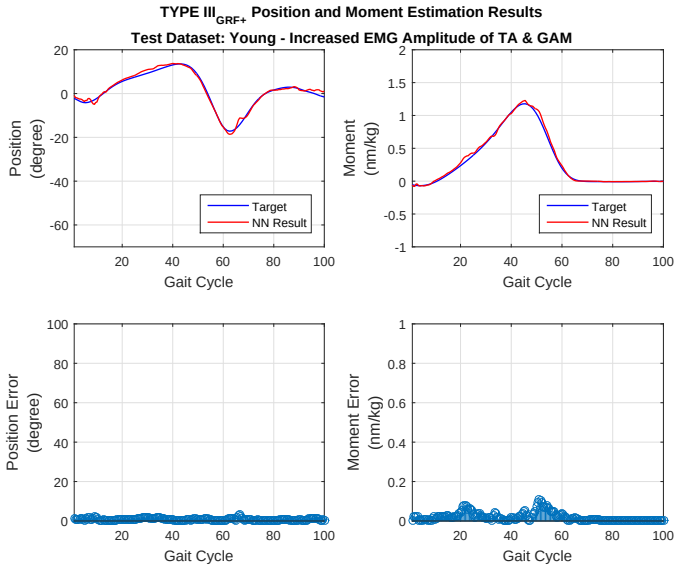

Figure A.69 TYPE III$_{GRF+}$ output when the 'Increased EMG Amplitude of TA and GAM' speed class dataset of 'Young' age group is given as input.

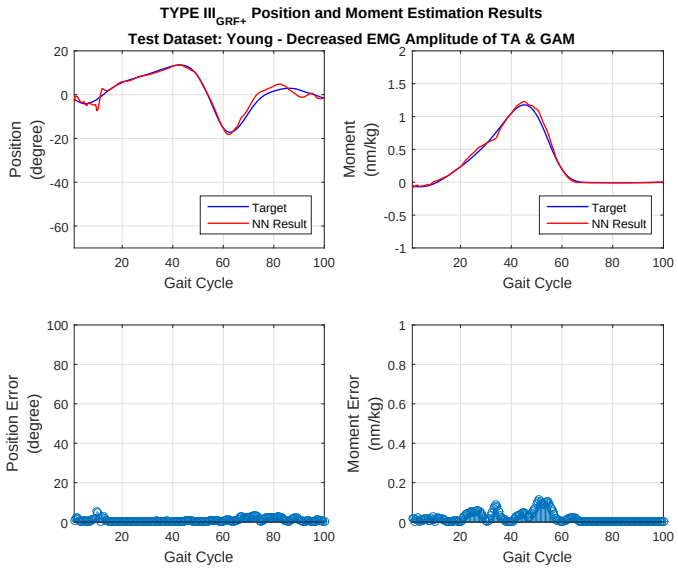

Figure A.70 TYPE III$_{GRF+}$ output when the 'Decreased EMG Amplitude of TA and GAM' speed class dataset of 'Young' age group is given as input.

REFERENCES

1. Seymour, R., *Prosthetics and Orthotics: Lower Limb and Spinal*, Philadelphia: Lippincott, Williams and Wilkins, 2002.

2. Eilenberg, M. F., H. Geyer, and H. Herr, "Control of a powered ankle-foot prosthesis based on a neuromuscular model," *IEEE Transactions on Neural Systems and Rehabilitation Engineering*, Vol. 18, April 210.

3. Winter, D. A., "Biomechanical motor patterns in normal walking," *Journal of Motor Behavior*, Vol. 15, January 1984.

4. Palmer, M. L., "Sagittal plane characterization of normal human ankle function across a range of walking gait speeds," Master's thesis, Massachusetts Institute of Technology, 2002.

5. Gates, D. H., "Characterizing ankle function during stair ascent, descent, and level walking for ankle prosthesis and orthosis design," Master's thesis, Boston University, 2004.

6. Tucker, M. R., J. Olivier, A. Pagel, H. Bleuler, M. Bouri, O. Lambercy, J. del R MillÃ¡n, R. Riener, H. Vallery, R. Gassert, R. Riener, H. Vallery, and R. Gassert, "Control strategies for active lower extremity prosthetics and orthotics: A review," *Journal of Neuroengineering and Rehabilitation*, Vol. 12, no. 1, 2015.

7. Au, S., P. Bonato, and H. Herr, "An emg-position controlled system for an active ankle-foot prosthesis an initial experimental study," *IEEE*, July 2005.

8. Au, S., M. Berniker, and H. Herr, "Powered ankle-foot prosthesis to assist level-ground and stair-descent gaits," *Neural Networks*, Vol. 21, March 2008.

9. Fleischer, C., and G. Hommel, "A human-exoskeleton interface utilizing electromyography," *IEEE Transcations on Robotics*, Vol. 24, August 2008.

10. Cavallaro, E. E., J. Rosen, J. C. Perry, and S. Burns, "Real-time myoprocessors for a neural controlled powered exoskeleton arm," *IEEE Transcations on Biomedical Engineering*, Vol. 53, November 2006.

11. Hoozemans, M. J. M., and J. H. van Dieen, "Prediction of handgrip forces using surface emg of forearm muscles," *Journal of Electromyography and Kinesiology*, Vol. 15, pp. 358–366, 2005.

12. Hill, A. V., "The heat of shortening and dynamics constants of muscles," in *Proceedings of the Royal Society of London. Series B, Biological Sciences*, Vol. 216, pp. 136–195, Royal Society, 1938.

13. Naidu, D. S., C.-H. Chen, A. Perez, and M. P. Schoen, "Control strategies for smart prosthetic hand technology: An overview," *30th Annual International IEEE EMBS Conference*, August 2008.

14. Sepulveda, F., D. M. Wells, and C. L. Vaughan, "A neural network representation of electromyography and joint dynamics in human gait," *Journal of Biomechanics*, Vol. 26, pp. 101–109, February 1993.

15. Savelberg, H. H. C. M., and W. Herzog, "Prediction of dynamic tendon forces from electromyographic signals: An artificial neural network approach," *Journal of Neuroscience Methods*, Vol. 78, pp. 65–74, 1997.

16. Liu, M. M., W. Herzog, and H. H. C. M. Savelberg, "Dynamic muscle force predictions from emg: An artificial neural network approach," *Journal of Electromyography and Kinesiology*, Vol. 9, pp. 391–400, 1999.

17. Huang, H., T. A. Kuiken, and R. D. Lipschutz, "A strategy for identifying locomotion modes using surface electromyography," *IEEE Transactions on Biomedical Engineering*, Vol. 56, pp. 65–73, January 2009.

18. Zhang, Z., Z. Wang, J. Jiang, and J. Qian, "A method to control ankle exoskeleton with surface electromyography signals," *Journal of Shanghai University (English Edition)*, Vol. 13, pp. 270–273, August 2009.

19. Kiguchi, K., and Y. Hayashi, "An emg-based control for an upper-limb power-assist exoskeleton robot," *International Conference on Intelligent Robotics and Applications (ICIRA) 2010: Intelligent Robotics and Applications*, pp. 390–397, 2012.

20. Sup, F., H. A. Varol, J. Mitchell, T. Withrow, and M. Goldfarb, "Design and control of an active electrical knee and ankle prosthesis," *2nd Biennial IEEE/RAS-EMBS International Conference on Biomedical Robotics and Biomechatronics*, October 2008.

21. Konrad, P., *The ABC of EMG: A Practical Introduction to Kinesiological Electromyography*, Noraxon USA, Inc., 2005.

22. Inman, V. T., H. J. Ralston, and F. Todd, *Human Walking*, Baltimore, London: Williams and Wilkins, 1981.

23. Neumann, D. A., *Kinesiology of the Musculoskeletal System: Foundations for Rehabilitation, 2nd Edition*, Mosby Elsevier, 2015.

24. Shultz, S. J., P. A. Houglum, and D. H. Perrin, *Examination of Musculoskeletal Injuries, 3rd Edition*, North Carolina: Human Kinetics, 2005.

25. Loudon, J., M. Swift, and S. Bell, *The Clinical Orthopedic Assessment Guide, 2nd Edition*, Kansas: Human Kinetics, 2008.

26. Brunnekreef, J. J., C. J. T. van Uden, S. van Moorsel, and J. G. Kooloos, "Reliability of videotaped observational gait analysis in patients with orthopedic impairments," *BMC Musculoskeletal Disorders*, Vol. 6, March 2005.

27. Dicharry, J., "Kinematics and kinetics of gait from lab to clinic," *Clinics in Sports Medicine*, Vol. 29, pp. 347–364, July 2010.

28. Perry, J., and J. Burnfield, *Gait Analysis: Normal and Pathological Function, 2nd Edition*, Slack Incorporated, 1992.

29. Palastanga, N., and R. W. Soames, *Anatomy and Human Movement, 6th Edition*, Elsevier, 2011.

30. Winter, D. A., *The Biomechanics and Motor Control of Human Gait*, Ontario: University Of Waterloo, 1987.

31. Winter, D. A., and S. E. Sienko, "Biomechanics of below-knee amputee gait," *Journal of Biomechanics*, Vol. 21, no. 5, pp. 361–367, 1988.

32. Klodd, E., A. Hansen, S. Fatone, and M. Edwards, "Effects of prosthetic foot forefoot exibility on gait of unilateral transtibial prosthesis users," *Journal of Rehabilitation Research and Development*, Vol. 47, no. 9, pp. 899–910, 2010.

33. Brockett, C. L., and G. J. Chapman, "Biomechanics of the ankle," *Journal of Orthopaedic Trauma*, Vol. 30, pp. 232–238, June 2016.

34. Quinlivan, B. T., S. Lee, P. Malcolm, D. M. Rossi, M. Grimmer, C. Siviy, N. Karavas, D. Wagner, A. Asbeck, I. Galiana, and C. J. Walsh, "Assistance magnitude versus metabolic cost reductions for a tethered multiarticular soft exosuit," *Science Robotics*, Vol. 2, January 2017.

35. Robertson, G., G. Caldwell, J. Hamill, G. Kamen, and S. Whittlesey, *Research Methods in Biomechanics*, Human Kinetics, 2004.

36. Basmajian, J. V., *Muscles Alive: Their Functions Revealed by Electromyography*, Baltimore, London: Williams & Wilkins, 1985.

37. Sutherland, D. H., "The evolution of clinical gait analysis part 1: Kinesiological emg," *Gait and Posture*, Vol. 14, pp. 61–70, 2001.

38. Basmajian, J. V., C. A. Gowland, M. A. Finlayson, A. L. Hall, L. R. Swanson, P. W. Stratford, J. E. Trotter, and M. E. Brandstater, "Stroke treatment: Comparison of integrated behavioral-physical therapy vs traditional physical therapy programs," *Archives of Physical Medicine and Rehabilitation*, Vol. 68, no. 5, pp. 267–272, 1987.

39. Colombo, G., M. Wirz, and V. Dietz, "Driven gait orthosis for improvement of locomotor training in paraplegic patients," *Spinal Cord*, Vol. 39, no. 5, pp. 252–255, 2001.

40. Jimenez-Fabian, R., and O. Verlinden, "Review of control algorithms for robotic ankle systems in lower-limb orthoses, prostheses, and exoskeletons," *Medical Engineering and Physics*, Vol. 34, pp. 397–408, 2012.

41. Kandel, E. R., J. H. Schwartz, and T. M. Jessell, *The Biomechanics and Motor Control of Human Gait, 4th Edition*, New York : McGraw-Hill, Health Professions Division, 2000.

42. Luca, C. J. D., and Z. Erim, "Common drive of motor units in regulation of muscle force," *Trends in Neurosciences*, Vol. 17, no. 7, pp. 299–305, 1994.

43. Luca, C. J. D., "The use of surface electromyography in biomechanics," *Journal of Applied Biomechanics*, Vol. 13, pp. 135–163, 1997.

44. Heckman, C. J., and R. M. Enoka, "Motor unit," *Comprehensive Physiology*, Vol. 2, pp. 2629–2682, October 2013.

45. Fengjun, B., *Muscle Force Estimation and Fatigue Detection Based on SEMG Signals*. PhD thesis, National University of Singapore, 2013.

46. Marieb, E. N., *Human Anatomy Physiology, 9th Edition*, Pearson Inc., 2012.

47. Farina, D., and F. Negro, "Accessing the neural drive to muscle and translation to neurorehabilitation technologies," *IEEE Reviews in Biomedical Engineering*, Vol. 5, pp. 3–14, 2012.

48. Hargrove, L. J., K. Englehart, and B. Hudgins, "A comparison of surface and intramuscular myoelectric signal classification," *IEEE Transactions on Biomedical Engineering*, Vol. 54, pp. 847–853, May 2007.

49. Smith, L. H., and L. J. Hargrove, "Comparison of surface and intramuscular emg pattern recognition for simultaneous wrist/hand motion classification," *35th Annual International Conference of the IEEE EMBS*, 3-7 July 2013.

50. Luca, C. J. D., *Surface Electromyography: Detection and Recording*, Delsys Inc., 2002.

51. Raez, M. B. I., M. S. Hussain, and F. Mohd-Yasin, "Techniques of emg signal analysis: Detection, processing, classification and applications," *Biological Procedures Online*, Vol. 8, pp. 11–35, 2006.

52. Naeem, U. J., C. Xiong, and A. A. Abdullah, "Emg-muscle force estimation model based on back-propagation neural network," *2012 IEEE International Conference on Virtual Environments Human-Computer Interfaces and Measurement Systems (VECIMS) Proceedings*, pp. 222–227, 2012.

53. Gurney, K., *An Introduction to Neural Networks*, CRC Press, 1997.

54. Guyton, A. C., *Textbook of Medical Physiology, 7th Edition*, W. B. Saunders, 1986.

55. Krenker, A., J. Bester, and A. Kos, *Introduction to the Artificial Neural Networks*, INTECH Open Access Publisher, 2011.

56. Gonzalez-Ibarra, J. C., C. Soubervielle-Montalvo, O. Vital-Ochoa, and H. G. Perez-Gonzalez, "Emg pattern recognition system based on neural networks," *11th Mexican International Conference on Artificial Intelligence: Advances in Artifical Intelligence and Applications*, December 2012.

57. Alpaydin, E., *Introduction to Machine Learning, 2nd edition*, The MIT Press, 2011.

58. Mitchell, T. M., *Machine Learning*, Mcgraw-Hill, 1997.

59. Rumelhart, D. E., G. E. Hinton, and R. J. Williams, "Learning representations by back-propagating errors," *Nature*, Vol. 323, pp. 533–536, October 1986.

60. Li, Y., Y. Fu, H. Li, and S.-W. Zhang, "The improved training algorithm of back propagation neural network with self adaptive learning rate," *2009 International Conference on Computational Intelligence and Natural Computing*, June 2009.

61. Mohri, M., A. Rostamizadeh, and A. Talwalkar, *Foundations of Machine Learning*, The MIT Press, 2012.

62. Rojas, R., *Neural Networks - A Systematic Introduction*, Springer, 1996.

63. Karlik, B., M. O. Tokhi, and M. Alci, "A fuzzy clustering neural network architecture for multifunction upper-limb prosthesis," *IEE Transactions on Biomedical Engineering*, Vol. 50, November 203.

64. Bovi, G., M. Rabuffetti, P. Mazzoleni, and M. Ferrarin, "A multiple-task gait analysis approach: Kinematic, kinetic and emg reference data for healthy young and adult subjects," *Gait and Posture*, Vol. 33, pp. 6–13, 2011.

65. MacKay, D. J. C., "A practical bayesian framework for backpropagation networks," *Computation and Neural Systems*, Vol. 4, pp. 448–472, 1992.

66. Vilimek, M., "An artificial neural network approach and sensitivity analysis in predicting skeletal muscle forces," *Acta of Bioengineering and Biomechanics*, Vol. 16, no. 3, 2014.

67. Farry, K. A., "Myoelectric teleoperation of a complex robotic hand," *IEEE Transactions on Robotics and Automation*, Vol. 12, no. 5, pp. 775–788, 1996.

68. Zhang, Z., J. Jiang, L. Peng, and H. Fan, "A method to control ankle exoskeleton with surface electromyography signals," *Journal of Shanghai University (English Edition)*, Vol. 13, pp. 270–273, August 2010.

69. Rahmatian, S., M. J. Mahjoob, and M. R. Hanachi, "Continuous estimation of anlle joint angular position based on the myoelectric signals," *Artificial Intelligence and Robotics*, 2016.

70. Wang, L., and T. S. Buchanan, "Prediction of joint moments using a neural network model of muscle activations from emg signals," *IEEE Transactions on Neural Systems and Rehabilitation Engineering*, Vol. 10, March 2002.